Ab Initio Free Energies of Adsorption from Anharmonic Vibrations

DISSERTATION

zur Erlangung des akademischen Grades
Doctor rerum naturalium
(Dr. rer. nat.)

im Fach Chemie

eingereicht an der

Mathematisch-Naturwissenschaftlichen Fakultät
der Humboldt-Universität zu Berlin

von

Herrn Dipl. Chem. GiovanniMaria Piccini

Präsident der Humboldt-Universität zu Berlin
Prof. Dr. paed. Jan-Hendrik Olbertz

Dekan der Mathematisch-Naturwissenschaftlichen Fakultät
Prof. Dr. Elmar Kulke

Gutachter:

1. Prof. Dr. Joachim Sauer
2. Prof. Dr. Claudia Draxl
3. Prof. Piero Ugliengo

Tag der mündlichen Prüfung: 23. April 2015

Abstract

The thermodynamic of adsorption is investigated from the vibrational point of view using quantum chemical methods via statistical mechanics. Due to the lack of accuracy of the present available methods for investigating periodic systems, such as plane-wave density functional theory (DFT), a novel computational strategy is presented to overcome these limitations and bring the estimate of the thermodynamic functions within chemical accuracy limits. The protocol presented in this work consists of different computational steps, namely a structure optimization using normal mode coordinates instead of Cartesians, a numerical harmonic frequency calculation via sampling of the potential energy surface along the normal mode coordinates and the inclusion of anharmonic correction to the latter. The normal mode coordinate optimization ensures a proper relaxation of the structure and a reliable set of real harmonic frequencies while the anharmonic corrections account for a proper description of the vibrational structure of a system characterized by a very flat potential energy surface. Parallel to these calculations the electronic part of the adsorption energy is corrected using a hybrid QM:QM scheme to account the electronic correlations effects more accurately than DFT. The hybrid electronic adsorption energy and the vibrational thermal contributions obtained using anharmonic corrections are finally combined to get accurate estimate of the adsorption thermodynamic functions.

This protocol has been applied to two benchmark cases, the adsorption of methane in acidic chabazite (H-CHA, a zeolite) at 303 K, 0.1 MPa, θ =0.5, and the adsorption of methane on the flat (001) MgO surface at 47 K, 1.3×10^{-14} MPa, θ =1. These two studies show with evidence that using standard computational methodologies to investigate such types of adsorption, where the driving forces are mainly van der Waals interactions, lead to huge deviations of the results from the experimental values. Moreover, they confirm that the harmonic approximation fails completely in describing these specific situations as the model on which it relies does not represent the physical reality of the problem. Application of anharmonic corrections, derived by proper sampling of the PES using curvilinear displacements along the normal modes (linear combinations of internal coordinates), proved to be able in describing properly the vibrational structure of the system and the consequences of this on the thermodynamics. The results for the calculated Gibbs free energy of

adsorption of the two systems deviate from the experiment by 2.3 kJ/mol and 2.1 kJ/mol for methane in H-CHA and methane on MgO(001), respectively, all within chemical accuracy. Furthermore, the adsorption in H-CHA has been extended to the case of ethane and propane at 313 K, 0.1 MPa, θ =0.5. The calculated thermodynamics functions show with evidence that the harmonic model deviates strongly from the experimental results, especially the entropic term, $-T\Delta S$. The inclusion of anharmonic effects confirms that the improvement of the vibrational model enhances the accuracy of the thermodynamic functions estimate. The calculated Gibbs free energy of adsorption deviate by -3.2 kJ/mol, and -2.2 kJ/mol from the experimentally measured ones for ethane and propane, respectively. The calculation of the Gibbs free energies showed that the adsorption of propane is thermodynamically favored when the molecule is bound to the acidic site via primary carbon while the adsorption via secondary carbon one is strongly disfavored. The calculations show that the origin of this thermodynamic instability of secondary carbon adsorption is purely entropic as the enthalpy does not change significantly upon different adsorption configurations. These results are all in agreement with the experimental data within chemical accuracy and allow a deeper understanding of the associated processes.

Zusammenfassung

Die Thermodynamik von Adsorptionsvorgängen wurde mittels quantenchemischer Methoden und der statistischen Thermodynamik untersucht. Eine neue rechentechnische Methode wird vorgestellt, die den Mangel an Genauigkeit vorhandener Methoden zur Untersuchung periodischer Systeme, wie z. B. der Dichte-Funktional-Theorie, behebt, und es ermöglicht thermodynamische Funktionen mit chemischer Genauigkeit zu bestimmen. Das im Rahmen dieser Arbeit entwickelte Protokoll besteht aus verschiedenen rechentechnischen Schritten, als da wären, eine Strukturoptimierung in Normalkoordinaten anstatt in kartesischen Koordinaten, eine numerische Berechnung der harmonischen Frequenzen durch Abtasten der Potentialenergieoberfläche entlang der Normalkoordinaten und anschließender anharmonischer Korrektur. Die Normalkoordinatenoptimierung garantiert eine korrekte Relaxation der Struktur mit ausschließlich reellen harmonischen Frequenzen. Die anharmonischen Korrekturen ermöglichen eine gute Beschreibung der Schwingungsstrukturen von Systemen die durch eine besonders Flache PES gekennzeichnet sind. Gleichzeitig, wird durch die Verwendung eines QM: QM-Hybridverfahrens zur Bestimmung des elektronischen Anteils der Adsorptionsenergie eine höhere Genauigkeit in der Bestimmung der Korrelationsenergie im Vergleich zu DFT garantiert. Der elektronische Anteil der Adsorptionsenergie, sowie der Schwingungsthermische Anteil werden abschließend kombiniert um einen genauen Wert der thermodynamischen Funktionen zu erhalten.

Das vorgestellte Protokoll wurde auf zwei Testfälle angewendet, der Methanadsorption in saurem Chabazite (H-CHA, ein Zeolith) bei 303 K, 0.1 MPa, θ =0.5, und der Adsorption von Methan auf der perfekten MgO (001) Oberfläche bei 47 K, 1.3×10^{-14} MPa, θ =1. Diese zwei Testfälle belegen, dass die Nutzung rechenbasierter Standartverfahren zu großen Abweichungen zwischen Theorie und Experiment in der Beschreibung von Adsorptionsvorgängen basierend auf Van-der-Waals-Wechselwirkungen führen kann. Es zeigt sich außerdem, dass die harmonische Näherung komplett versagt in der Beschreibung dieser spezifischen Vorgänge, da das ihr zugrunde liegende Modell nicht der physikalischen Realität entspricht. Die Anwendung der anharmonischen Korrekturen, abgeleitet aus einem genauen abtasten der PES mittels Auslenkung entlang der Normalmoden (Linearkombinationen von internen Koordinaten) in “curvi-

lineare" Koordinaten, liefern eine gute Beschreibung der Schwingungsstruktur und den sich daraus ergebenen thermodynamischen Konsequenzen. Die so bestimmten freien Gibbs-Adsorptionsenergien weichen um 2.3 kJ/mol Adsorption von Methan in H-CHA bzw. 2.1 kJ/mol Adsorption von Methan auf MgO(001) von den experimentell bestimmten Werten ab. Die Abweichungen liegen somit im Bereich chemischer Genauigkeit. Des Weiteren wurde die Adsorption von Ethan und Propan in H-CHA bei 303 K, 0.1 MPA, θ =0.5 untersucht. Die berechneten thermodynamischen Funktionen belegen, dass das harmonische Modell (die harmonische Näherung) versagt und es dadurch zu großen Abweichungen im Vergleich zu den experimentellen Daten kommt, speziell in dem Entropieterm $-T\Delta S$. Die Berücksichtigung anharmonischer Korrekturen bestätigt, dass die Verbesserung des zugrunde liegenden Schwingungsmodells die Genauigkeit der thermodynamischen Funktionen erhöht. Die berechneten freien Gibbs-Adsorptionsenergien weichen um -3.2 kJ/mol Adsorption von Ethan bzw. -2.2 kJ/mol Adsorption von Propan von den experimentell bestimmten Werten ab. Im Fall der Adsorption von Propan konnte anhand der freien Gibbs-Adsorption Energie gezeigt werden, dass die Adsorption am aciden H-Atom via des primären Kohlenstoffatoms thermodynamisch bevorzugt ist, während die Adsorption über das sekundäre Kohlenstoffatom thermodynamisch stark benachteiligt ist. Die Untersuchung ergab, dass der Ursprung dieser verschieden Stabilitäten völlig auf entropischen Effekten beruht, während sich keine oder nur kleine Unterschiede in den Adsorptions-Enthalpien. Diese Ergebnisse stimmen alle, im Rahmen chemischer Genauigkeit, mit den experimentellen Resultaten überein und erlauben somit ein tieferes Verständnis des zu Grunde liegenden Prozesses.

Publications

This thesis is based on three publications/manuscripts

1. G. Piccini and J. Sauer, "Quantum chemical free energies: Structure optimization and vibrational frequencies in normal modes," *J. Chem. Theory Comput.*, vol. 9, no. 11, pp. 5038–5045, 2013

2. G. Piccini and J. Sauer, "Effect of anharmonicity on adsorption thermodynamics," *J. Chem. Theory Comput.*, vol. 10, no. 6, pp. 2479–2487, 2014

3. G. Piccini, M. Alessio, J. Sauer, Y. Zhi, Y. Liu, R. Kolvenbach, A. Jentys, and J. A. Lercher, "Accurate adsorption thermodynamics of small alkanes in zeolites. ab initio theory and experiment for h-chabazite," *J. Phys. Chem. C*, vol. 119, pp. 6128–6137, 03 2015

Contents

1 Introduction

1.1 Motivation

A quantitative theory of heterogeneous catalysis requires accurate knowledge of thermodynamic functions for all elementary reaction steps, adsorption, chemical transformations, and desorption steps. Statistical thermodynamics relates rate and equilibrium constants to free energy changes for the formation of activated complexes (transition state theory) and for the product formation, respectively [4]. While it has been demonstrated that energy barriers and reaction energies for large chemical systems such as enzymes [5], zeolites [6–8], and metal-organic frameworks [9, 10] can be predicted with chemical accuracy ($\pm$ 1 kcal/mol $\approx \pm$ 4.2 kJ/mol), the ab initio prediction of free energy changes is more challenging. Sampling the potential energy surface by molecular dynamics [11–13] e.g. umbrella sampling or thermodynamic integration requires millions of time steps to reach convergence. This limits these methods to cases for which good force fields are available, which is often the case in molecular biology, but for molecule - surface interactions force fields that describe both adsorption and reaction steps with sufficient accuracy for free energy simulations are not available.

The alternative approach, calculating free energies from vibrational partition functions, relies on the expansion of the high-dimensional potential energy surface around the stationary points (minimum or transition structure) and is standard for molecular systems. Provided that the harmonic approximation is made, it becomes tractable even for system with hundreds of atoms and it has been applied to surface reactions [7] and adsorption processes [10, 14–17]. When density functional theory (DFT) is applied to large systems (unit cells in the periodic case), as required for realistic periodic models of active sites for surface reactions, e.g. in zeolites, force constants have to be calculated by numerical derivatives of analytically calculated forces. While the force constants can be cal-

culated directly from the ab initio potential energies without fitting, the main limitation of the harmonic oscillator model is that small vibrational frequencies make the largest contribution to the entropies and that relatively small errors on these frequencies lead to large errors in the entropy term. Since soft, low frequency modes are characteristic of molecule - surface interactions, both the determination of the energy minimum structure and the numerical differentiation face accuracy limits when applying DFT codes designed for large scale calculations under periodic boundary conditions and using plane waves, such as VASP [18]. This has been also observed in previous applications of plane wave codes, e.g. in calculations of phonons for molecular crystals[19]. This is particularly true for the low frequency modes arising from molecule - surface interactions (three translational and three rotational degrees of freedom are converted into six molecule - surface vibrations, i.e. in more or less *hindered* translations and rotations) and soft vibrational modes of the solid material, e.g. in zeolite frameworks [20–23]. Here it is shown that chemical accuracy can be reached for free energies provided that a re-optimization step is applied using different coordinates, normal mode coordinates instead of Cartesians, and that anharmonic vibrational frequencies are calculated for each of the normal modes separately [1, 2, 24] and the potential is evaluated for curvilinear distortions [2] as suggested by Gordon and coworkers for molecules [25–29].

In the area of adsorption and catalysis, development and validation of new computational protocols is hampered by the scarcity of reliable experimental data for comparison with the results. The present work aims at extending the list of thermodynamic reference systems by proving computational thermodynamic benchmark data for the adsorption of methane, ethane, and propane in the acidic zeolite chabazite, H-SSZ-13, and of methane on the MgO(001) surface. Due to its limited unit cell size the chabazite framework is well-suited for computational studies [1, 2, 6, 30–33] and its aluminum phosphate form is industrially used as a catalyst in hydrocarbon synthesis processes [34–36]. MgO(001) is the thermodynamically most stable surface of MgO and represents a good model for adsorption of molecules on the MgO(001) terrace sites in real catalysts. The adsorption of methane on this surface has been matter of both experimental [37–43] and computational studies [44]. It will be shown that chemical accuracy is reached for both heats and free energies of adsorption provided the energies are calculated ab initio with a hybrid

high-level low level quantum mechanics scheme and the vibrational partition functions are calculated from anharmonic vibrational frequencies. The latter are obtained from the curvilinear sampling of one-dimensional potentials for each degree of freedom.

1.2 Adsorption Thermodynamics

In modeling a surface reaction mechanism, three processes have to be taken into account: adsorption, the reaction step and desorption. Figure 1.1 shows a schematic representation of such a process with the four fundamental thermodynamic states involved. The mechanism of a unimolecular surface reaction can be easily described as follows. First, a molecule from the gas phase (g) approaches a surface site (in case of catalysts an active site) that is in the solid state (s) and forms an adsorption complex. Subsequently, the complex reacts and forms the product that is still adsorbed on the surface. When such a molecule desorbs, the products are released into the gas phase. What is very important to notice is that the adsorbed molecule changes its phase. It goes from the gas phase state having 3 translational degrees of freedom, 3 rotational ones (or 2 in the case of a linear molecule) and 3N-6(5) vibrational ones to the solid phase when the adsorption complex is formed in which all the translations and rotations are formally interconverted into vibrational degrees of freedom of the whole system. Of course this is a considerably rough approximation as the vibrations associated with the former translational and rotational degrees of freedom still retain part of their character. They are usually classified as *frustrated* or *hindered* translations and rotations in the case of chemisorption and physisorption, respectively. In this work, the attention is focused on the molecular adsorption (no bond rearrangement, see refs. [45, 46]) of organic molecules (alkanes) on inorganic surfaces such as zeolites or magnesium oxide. Typically the forces involved in molecular adsorption are van der Waals type forces [47, 48]. This means that the electronic structure perturbation of the whole system upon adsorption is small or, in other words, that the adsorbed molecules moves on a rather flat potential. The outcome is that the *hindered* translations and rotations of the adsorbed molecule are less constraint.

These circumstances have a drastic impact on the evaluation of the thermodynamics functions from the statistical mechanics approach, i.e. from

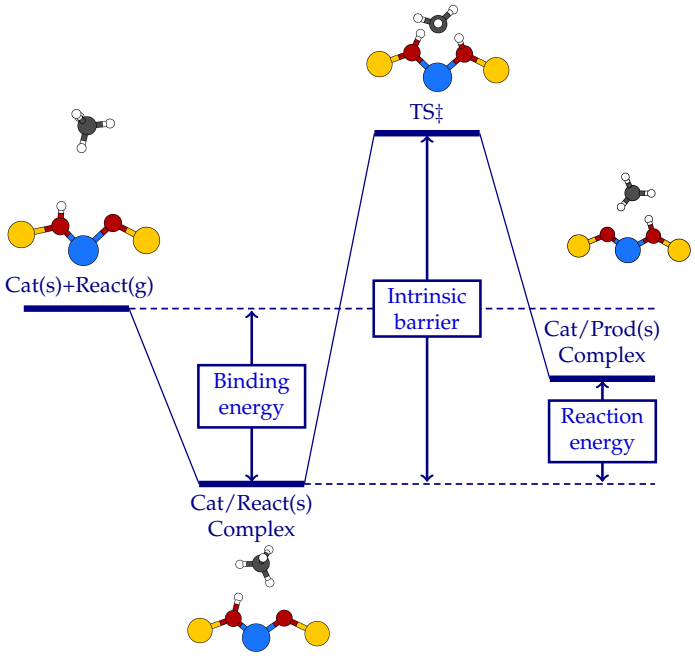

Figure 1.1: *Surface reaction energy scheme showing the pre-adsorbed state, reactants adsorption, transition state, and product adsorption.*

the translational, rotational, and vibrational partition functions. Assuming that the free particle and free rotor model represent a good approximation for the gas phase molecule translational and rotational partition functions [49] more care should be given when adopting a purely harmonic model to treat the vibrational degrees of freedom. This can be illustrated considering the dependency of the internal energy and the entropy term for a system of 3N-3 oscillators on the frequency. The general expression for the vibrational internal energy is

$$E_v = R \sum_{j}^{3N-3} \left[\frac{h\nu_j}{k_B \left(e^{\frac{h\nu_j}{k_B T}} - 1 \right)} \right] \tag{1.1}$$

and for the entropy term

$$TS_\nu = R \sum_j^{3N-3} \left[\frac{h\nu_j}{k_B \left(e^{\frac{h\nu_j}{k_b T}} - 1 \right)} - k_B T \log \left(1 - e^{-\frac{h\nu_j}{k_B T}} \right) \right] \tag{1.2}$$

Where T is the temperature, R the ideal gas constant, h the Planck constant, k_B the Boltzmann constant and ν_j the harmonic frequency of the j-th oscillator. Taking the limit of zero approaching frequencies for a generic oscillator j, some interesting results are obtained. The first term is equal both for internal energy and for the entropy term. Expanding the Boltzmann factor in Taylor series and taking the limit $\nu_j \to 0$ the result is

$$\begin{aligned} \lim_{\nu_j \to 0} R \left[\frac{h\nu_j}{k_B \left(e^{\frac{h\nu_j}{k_b T}} - 1 \right)} \right] &= \lim_{\nu_j \to 0} R \left[\frac{h\nu_j}{k_B \left(1 + \frac{h\nu_j}{k_B T} + \frac{1}{2!} \left(\frac{h\nu_j}{k_B T} \right)^2 + \cdots - 1 \right)} \right] \\ &= \lim_{\nu_j \to 0} R \frac{h\nu_j}{\frac{h\nu_j}{T}} \\ &= RT \end{aligned} \tag{1.3}$$

Thus, for each frequency approaching zero, the contribution to the internal energy is RT which is what one would expect for a translational degree of freedom since $\nu_j = 0$ means that the oscillating mass is moving in a potential that is zero everywhere, i.e. a free particle. A more interesting and still physically consistent result is the outcome of the limit of the logarithmic term in the right hand side of eq. 1.2. Expanding again in Taylor series, the limit is

$$\begin{aligned}\lim_{\nu_j\to 0} k_B T \log\left(1-e^{-\frac{h\nu_j}{k_B T}}\right) &= \lim_{\nu_j\to 0} k_B T \log\left(1-1+\frac{h\nu_j}{k_B T}-\frac{1}{2!}\left(\frac{h\nu_j}{k_B T}\right)^2+\dots\right)\\ &= \lim_{\nu_j\to 0} k_B T \log\left(\frac{h\nu_j}{k_B T}\right)\\ &= -\infty\end{aligned} \tag{1.4}$$

Thus, the entropic term will diverge to infinity when the limit of zero frequency is reached. This is again in agreement with the physical picture. A zero frequency or zero potential means that the mass is free to span the whole space from $-\infty$ to $+\infty$ in each direction. From a statistical point of view, the particle can be found equally likely everywhere in the infinite space. Therefore, the disorder is maximal or, in other words, the entropy of the system is infinite [4].

Many chemical systems are characterized by low frequency modes (e.g. *hindered* translations and rotations) which therefore contribute largely to the vibrational entropy. This means that even small inaccuracies in the evaluation of the vibrational frequencies lead to a huge propagation of the errors in the estimation of the vibrational entropy. As it will be shown later, the main goal of this work is to improve the accuracy in the calculation of the vibrational structure in adsorption related phenomena to achieve chemical accuracy in entropy estimation.

1.3 Systems of Interest

Adsorption is a typical interface phenomenon which involves in principle every kind of material surface. Beside the academical interest in this extremely challenging field that combines efficiently physics and chemistry points of view, there is a wide technological and industrial research effort focused on the application of adsorbent materials [50–53]. These materials span a large range of chemical structures and composition going from carbon based materials [54] to organic/inorganic materials such as metal organic frameworks (MFOs) [52, 55–60], a large variety of metal oxides (see e.g. [61–64]), and wide panorama of zeolites of different topologies,

structure and composition. In this work the adsorption in acidic zeolites is the main subject of study beside an investigation of adsorption on the magnesium oxide (001) surface. In the following subsections, the main structural and chemical features of the studied materials are presented.

1.3.1 Magnesium Oxide

Magnesium oxide is know to have acid-base properties and for this it is largely used in catalysis both as an active catalyst [65] or as a support [66]. It is a ionic solid formed by Mg^{2+} and O^{2-} ions. This material is employed in many technological applications ranging from construction to opto-electronics. It can be easily produced by direct oxidation in air atmosphere of magnesium metal (smoke MgO). In this work, a clean (001) MgO surface is taken into account as it can be synthesized on support via epitaxial growth (see e.g. ref. [67]). Studying the adsorption thermodynamics of hydrocarbons on the MgO(001) surface [38] is a fundamental step in understanding the catalytic properties of this material. In the last years, MgO became one of the best eligible catalysts for the oxidative coupling of methane (OCM) reaction [68–70]. Therefore, a detailed atomistic point of view of the adsorption structures and thermodynamics is very important as the reactions take place in the gas phase. Many experimental works have been carried out regarding the structure and other properties of methane monolayers on the MgO(001) surface [38–43], elucidating the main features of this particular adsorption arrangement.

1.3.2 Zeolites

Zeolites are a class of natural and synthetic materials formed by corner-sharing SiO_2 tetrahedral units. These corner-sharing tetrahedra can form 4-, 5-, 6-, 7-, 8-, 10-, or 12-membered rings which are the building blocks of every zeolite topology (see refs. [71, 72]). Such building blocks can combine giving rise to cage-like structures which are further bound together giving rise to complex 3D arrangements such as windows, pores, and channels. For this reason, zeolites are classified as nanoporous materials since their microscopic atomic arrangement is such that most of the crystal volume is vacuum space. In fact, zeolites have a relatively low density and very high specific surface area. Basically most of the inner surface of zeolites is available. Purely siliceous zeolites are poor adsorbents and

have no catalytic activity. The most important feature combining sinergically with the specific nanoporous structure of zeolites is that Si atoms can be substituted with an Al atom. Since Al atoms have one valence electron less than Si atoms, the substitutional defect has a formal charge corresponding to -1. In most of the natural zeolites, this charge is counterbalanced by an alkali ion such as Na^+ or K^+ which are poorly bound to the defect site. Such materials are used as adsorbents and also as catalysts [73], but their main use is as ion-exchangers for water or soil purification from pollutants or nuclear waste. Outstanding catalytic activities of zeolites are reached when the alkali ion is substituted by a proton through hydrolization. The result is that the zeolite becomes a solid Brønsted acid. The adsorbent and catalytic properties of these materials have been matter of many studies since many years as they can be synthesized in many different crystal structures and with various aluminum contents in order to obtain an efficient catalyst with tunable properties. Zeolites structure is such that they can be selective with respect to reactants and products [74]. For this reason, they are also addressed as "molecular sieves" as they can separate gas molecules with respect to their molecular volume or structure [74–78].

In this work, the zeolite framework considered is the acidic chabazite (referred as H-CHA or H-SSZ-13). This type of framework can be found in nature [79, 80] and also synthesized [81]. The chabazite framework consists to stacked double 6-ring sequences that give rise to an ellipsoidal cage-like structure as shown in Figure 1.2.

There are two types of channels. The largest are confined by the 8-membered rings (in blue Fig. 1.2) and the smallest are confined by the 6-membered rings (in red Fig. 1.2). The gas phase molecules can diffuse through the crystal structure along these channels and adsorb on the Brønsted sites.

Chabazite showed particular catalytic properties in its protonated form [34] or in some ion-exchanged forms (e.g. Cu [82]). Moreover, chabazite isostructural silicoaluminophosphate (SAPO) [35] can be synthesized having particular catalytic properties. Despite these materials are extremely interesting, they have not been taken into account in this work.

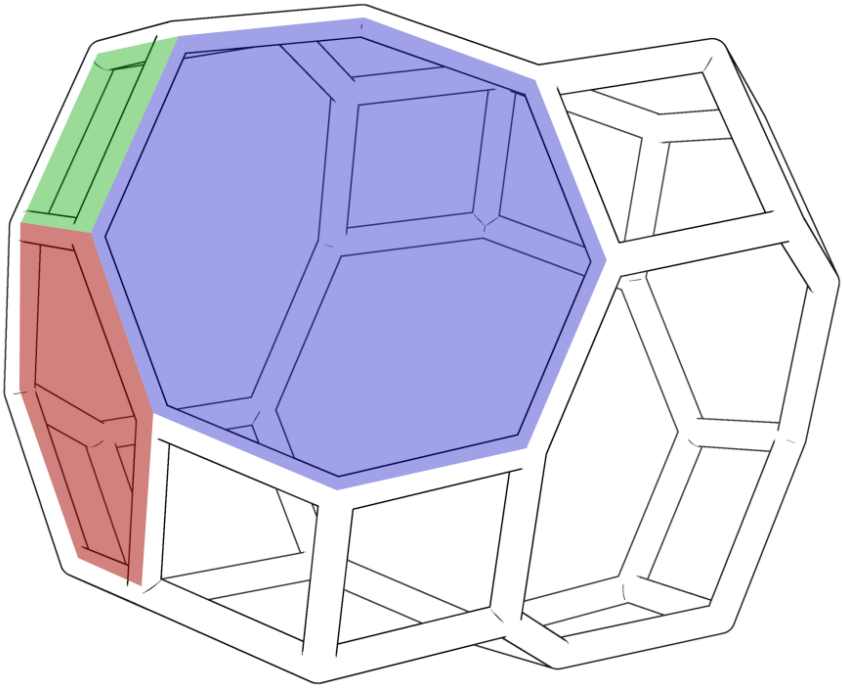

Figure 1.2: *Schematic representation of chabazite ellipsoidal cage showing connection between Si or Al atoms (T-sites). Color key: blue - 8-membered ring, red - 6-membered ring, green - 4-membered ring.*

2 Methods

2.1 The Born-Oppenheimer Approximation

The Born-Oppenheimer (BO) approximation is central to quantum chemistry. It reduces the complexity in solving the molecular Schrödinger equation introducing a quantitative separation of the electronic and nuclear variables. It is based on the difference in mass between electrons and nuclei ($\sim 10^3 - 10^5$). Since the nuclei are more massive, their motion is relatively slow with respect to electrons. The latter are therefore assumed to respond *instantaneously* to the motion of the nuclei. Here follows a simplified discussion of the BO approximation allowing the derivation of the fundamental concept of the potential energy surface.

The total non-relativistic Hamiltonian for a molecular system can be written as[1]

$$\begin{aligned} H = & \underbrace{-\sum_i \frac{1}{2m_i}\nabla_i^2}_{T_{nuc}} \\ & \underbrace{-\sum_\mu \frac{1}{2}\nabla_\mu^2 - \sum_{\mu,i} \frac{Z_i}{|\mathbf{r}_\mu - \mathbf{R}_i|} + \sum_{\mu,\nu} \frac{1}{|\mathbf{r}_\mu - \mathbf{r}_\nu|} + \sum_{i,j} \frac{Z_i Z_j}{|\mathbf{R}_i - \mathbf{R}_j|}}_{H_{el}} \end{aligned} \tag{2.1}$$

where the indices $i, j \ldots$ label the nuclei and $\mu, \nu, \ldots$ label the electrons. $\mathbf{R}_i$ and $\mathbf{r}_\mu$ are the nuclear and electronic coordinates, respectively. Z_i is the charge of the i-th nucleus and m_i its mass. The molecular Hamiltonian can be rewritten as a sum of two contributions as specified in eq. 2.1 where T_{nuc} is the kinetic energy operator of the nuclei and H_{el} is the

[1] Atomic units are used throughout the thesis unless directly specified.

electronic Hamiltonian. It must be noticed that the separation is not symmetric in electrons and nuclei since the nuclear repulsion term is embodied in the electronic Hamiltonian. However, since this term depends only on the nuclear coordinates and not on their derivatives as in T_{nuc}, it has the effect of a constant and the electronic Hamiltonian depends *parametrically* on it. Therefore, the electronic problem can be solved considering the nuclei fixed in space:

$$H_{el}(\mathbf{r};\mathbf{R})\psi_{el}(\mathbf{r};\mathbf{R}) = E_{el}(\mathbf{R})\psi_{el}(\mathbf{r};\mathbf{R}) \tag{2.2}$$

Note that the eigenvalue E_{el} of the above equation depends parametrically on the nuclear coordinates $\mathbf{R}$. Now the total wave function is approximated as a product

$$\Psi_{BO}(\mathbf{r};\mathbf{R}) = \psi_{nuc}(\mathbf{R})\psi_{el}(\mathbf{r};\mathbf{R}) \tag{2.3}$$

where $\psi_{nuc}(\mathbf{R})$ is a solution to the equation

$$[T_{nuc}(\mathbf{R}) + E_{el}(\mathbf{R})]\,\psi_{nuc}(\mathbf{R}) = E\psi_{nuc}(\mathbf{R}) \tag{2.4}$$

Applying the total Hamiltonian to the BO wave function, the result is

$$\begin{aligned} H\Psi_{BO}(\mathbf{r};\mathbf{R}) &= [H_{el} + T_{nuc}]\,\psi_{nuc}(\mathbf{R})\psi_{el}(\mathbf{r};\mathbf{R}) \\ &= \psi_{nuc}(\mathbf{R})H_{el}\psi_{el}(\mathbf{r};\mathbf{R}) + T_{nuc}\psi_{nuc}(\mathbf{R})\psi_{el}(\mathbf{r};\mathbf{R}) \\ &= \psi_{nuc}(\mathbf{R})E_{el}(\mathbf{R})\psi_{el}(\mathbf{r};\mathbf{R}) + \psi_{el}(\mathbf{r};\mathbf{R})T_{nuc}\psi_{nuc}(\mathbf{R}) \\ &\quad -\sum_i \frac{1}{2m_i}\left[\psi_{nuc}(\mathbf{R})\nabla_i^2\psi_{el}(\mathbf{r};\mathbf{R}) + 2\nabla_i\psi_{nuc}(\mathbf{R})\nabla_i\psi_{el}(\mathbf{r};\mathbf{R})\right] \end{aligned} \tag{2.5}$$

It is clear that the electronic wave function still depends on the nuclear coordinates as the nuclear kinetic energy operator applies to it. However, this dependence (embodied in the last sum of eq. 2.5) is usually insignificant since each term is multiplied by $1/2m_i \approx 10^{-3} - 10^{-5}$. This means that the electronic wave function varies little upon small changes in the nuclear coordinates and the terms containing ∇_i and ∇_i^2 applied to $\psi_{el}(\mathbf{r};\mathbf{R})$ can be neglected, thus:

$$\begin{aligned} H\Psi_{BO}(\mathbf{r};\mathbf{R}) &\approx \psi_{el}(\mathbf{r};\mathbf{R})\left[T_{nuc} + E_{el}(\mathbf{R})\right]\psi_{nuc}(\mathbf{R}) \\ &= \psi_{el}(\mathbf{r};\mathbf{R})E\psi_{nuc}(\mathbf{R}) \\ &= E\Psi_{BO}(\mathbf{r};\mathbf{R}) \end{aligned} \tag{2.6}$$

The errors introduced by the BO approximation are in most of the cases very small, therefore the solutions of eq. 2.2 are considered as *exact*. It is fundamental to understand the parametric dependence of E_{el} on $\mathbf{R}$. Having a set of infinite or finite nuclear configuration $\{\mathbf{R}\}$, it is, thus, possible to construct a real or approximated potential energy surface respectively. Such a concept is the base of most of the discussions and derivations reported in this work as it provides the fundamental tool to calculate equilibrium structures and to derive different models to approximate ψ_{nuc}.

2.2 Walking on the Potential Energy Surface

The Potential Energy (hyper-)Surface (PES) is in most cases a multivariate function depending on a set of atomic coordinates $\{\mathbf{R}\}$. It is characterized by different types of stationary points, namely global or local maxima and minima and saddle points of different orders. Maxima, in general, do not correspond to interesting structures from the chemical point of view as they cannot be associated with a thermodynamic state. Minima and *first order* saddle points are way more interesting for chemistry. The firsts correspond to the equilibrium structures of the system as they represent the energetically favored configurations. They comprise all the possible stable structures of a generic molecular system, such as different isomers or reactants and products. Each minimum corresponds to a thermodynamic equilibrium state and can interconvert to another minimum passing through a transition state (TS). The structures associated with the TS, the transition structures, correspond to the first order saddle points connecting different minima along a minimum energy path [83]. Location and characterization of such points of the PES are fundamental to quantum chemistry as they allow the calculation of thermodynamic and kinetic parameters from the Eyring transition state theory [4, 84–86].

As mentioned above, the BO approximation introduces a parametric dependence of the electronic energy E on the nuclear coordinates $\mathbf{R}$. This

means that no analytical expression for $E(\mathbf{R})$ is available. Therefore, the local topology of the PES around a point $\mathbf{R}$ will be approximated using a model surface in order to study it. Many models have been proposed to approximate and subsequently minimize the PES going from first order approximation as in the steepest descend method to second order approximation as in the Newton method and its extensions [87]. Other minimization algorithms have been proposed for different purposes such as the conjugate-gradients method [88], generalized direct inversion of the iterative space (GDIIS) [89], genetic algorithm based search [90] and many others [91].

2.3 Normal Modes of Vibration

The concept of normal modes of vibration is fundamental to this work. The following section illustrates the mathematical origin of normal modes of vibration for a system of many oscillators following Wilson formalism [92].

For a generic molecular system, the vibrational Hamiltonian can be written in the harmonic approximation as

$$H = \frac{1}{2}\left(\Delta\dot{\mathbf{x}}^T\mathbf{M}\Delta\dot{\mathbf{x}} + \Delta\mathbf{x}^T\mathbf{H}\Delta\mathbf{x}\right) \tag{2.7}$$

where $\Delta\mathbf{x}$ is the vector of the Cartesian atomic displacements from the equilibrium position, $\mathbf{M}$ is the diagonal matrix of atomic masses ($M_{ij} = \delta_{ij}m_i$), $\mathbf{H}$ is the energy Hessian, i.e. the harmonic force constant, matrix. Index i goes from 1 to $3N$ counting each Cartesian $\{x, y, z\}$ degree of freedom per atom where N is the number of atoms in the system. Introducing mass-weighted coordinates $\mathbf{q} = \mathbf{M}^{\frac{1}{2}}\Delta\mathbf{x}$, the Hamiltonian transforms into

$$H = \frac{1}{2}\left(\dot{\mathbf{q}}^T\dot{\mathbf{q}} + \mathbf{q}^T\mathbf{f}\mathbf{q}\right) \tag{2.8}$$

where $\mathbf{f}$ is the mass-weighted Hessian matrix. Normal mode coordinates $\mathbf{Q}$ are defined as linear combination of mass-weighted coordinates

$$\mathbf{Q} = \mathbf{s}^T\mathbf{q}. \tag{2.9}$$

Imposing the orthogonality of the matrix $\mathbf{s}$ and defining a similarity trans-

formation of the Hessian

$$\mathbf{s}^T\mathbf{s} = \mathbf{1},\ \mathbf{s}^T\mathbf{f}\mathbf{s} = \mathbf{F},\ \text{where } F_{ij} = \delta_{ij}\omega_i^2 \tag{2.10}$$

the Hamiltonian can be written in diagonal form

$$H = \sum_{i=1}^{3N} \frac{1}{2}\left(\dot{Q}_i^2 + \omega_i^2 Q_i\right). \tag{2.11}$$

Thus a linear transformation between Cartesian and normal mode coordinates is defined

$$\Delta\mathbf{x} = \mathbf{M}^{-\frac{1}{2}}\mathbf{q} = \mathbf{M}^{-\frac{1}{2}}\mathbf{s}\mathbf{Q} = \mathbf{S}\mathbf{Q} \tag{2.12}$$

The resulting transformation matrix $\mathbf{S}$ is a matrix of eigenvectors $[\mathbf{v}_1, \mathbf{v}_2, \cdots, \mathbf{v}_{3N}]$ where each column corresponds to the cartesian coefficients of the linear combination for the k-th normal mode.

2.4 Calculation of the Hessian Matrix

To get the harmonic frequencies ω_i from eq. 2.10, the mass-weighted Cartesian Hessian is diagonalized. The latter is obtained by calculating the second derivative of the energy E (or the first derivative of the gradients). When analytical expressions of the potential energy are available (such as in molecular force fields), the calculation of the Hessian matrix is straightforward and does not require any approximation or numerical procedure. The iterative solution of the Hartree-Fock or Kohn-Sham equations yield an expression of the potential energy that directly depends on the molecular orbitals, i.e. on a linear combination of basis fucntions of different types. If local atomic centered Gaussian basis function are employed as a basis set (as in most common quantum chemical packages), second derivatives on the energy can be efficiently calculated iteratively from the solution of the self-consistent field (SCF) equation [93–95]. However, this efficiency depends directly on the basis set employed (Gaussian type functions) for which the Schwarz inequality [94] allows a pre-screening of some two-electron integrals that are not further calculated for the second derivative iterations. Unfortunately, basis sets such as plane waves due to their natural delocalization (no direct dependence

of the functions on the atomic coordinates) do not allow by construction the pre-screening. Moreover, the usual large dimension of the plane wave basis sets (up to several thousands of functions) makes the analytical calculation of the second derivatives without pre-screening completely unfeasible. The most practical solution to this problem is to compute the Hessian matrix numerically using a finite differences approach. To save computational time and gain accuracy, the calculation of the matrix is performed by first differentiation of the gradients that in the case of plane wave basis sets are analytical (Hellmann-Feynman forces)

$$H_{ij} = \frac{g_{x,i}(\Delta x_j) - g_{x,i}(-\Delta x_j)}{2\Delta x_j} \tag{2.13}$$

where $\mathbf{g_x}$ is the Cartesian gradient calculated at the distorted geometry $\boldsymbol{\Delta x}$. In this way it is possible to obtain an entire row of the Hessian matrix from two gradient calculations instead of calculating each element as it would be in the case of second derivative with respect to the energy. This way of calculating the Hessian matrix and therefore the eigenvalues (harmonic frequencies) and the eigenvectors (normal modes of vibration) have been employed throughout this work.

2.5 Structure Optimization in Normal Mode Coordinates

Once the transformation between Cartesian and normal mode coordinates is known (eq. 2.12), it can be used to perform a structure optimization directly along the normal modes of vibration. This structural refinement is fundamental when trying to get an accurate description of the vibrational structure of a chemical system, especially when one or more spurious imaginary frequencies are present. They key concept of the algorithm proposed first by Bouř and Keiderling [96] is the assumption that, in a region close to a stationary point, the normal modes of vibrational are completely decoupled. This assumption allows to produce a rational function optimization (RFO) [97] step along each normal mode

coordinate independently as follows

$$dQ_i^{new} = -\frac{2g_{Q,i}^{old}}{F_{ii} + \sqrt{F_{ii}^2 + 4(g_{Q,i}^{old})^2}} \tag{2.14}$$

where $\mathbf{g_Q} = \mathbf{S}^T\mathbf{g_x}$ is the gradient in normal mode coordinates. A new set of cartesian coordinates is obtained as

$$\mathbf{x}^{new} = \mathbf{x}^{old} + \mathbf{S}d\mathbf{Q}^{new} \tag{2.15}$$

Since at each time the coordinates change, also the second derivatives of the energy do, thus the Hessian matrix is updated using the Broyden-Fletcher-Goldfarb-Shanno (BFGS) formula [98] in this case which ensures the Hessian to be positive defined. If the stationary point of interest is a first order saddle point (i.e. a transition structure), other update schemes such as the Davidon-Fletcher-Powell (DFP) method [102] can be employed. Hessian update changes consequently the eigenvalues and eigenvectors defining relatively the entity of the optimization step and its direction. This is therefore a crucial and delicate point of the algorithm.

A Hessian matrix is needed from the beginning in order to define the coordinates transformation from cartesian to normal mode in eq. 2.14. In this work, the starting Hessian matrix is calculated numerically for the initially optimized structures and subsequently used as an initial guess to obtain the first eigenvalues and eigenvectors for the normal mode optimization. Prior to diagonalization, the Hessian matrix is projected to remove translational and/or rotational motions of the moving frame following the usual Eckart conditions [103].

2.6 Numerical Hessian in Normal Mode Coordinates

The most relevant source of error in the calculation of the harmonic frequencies via numerical differentiation is the type of displacement coordinates. If the displacements are done along each single atomic Cartesian coordinate with the same magnitude as in eq. 2.13, the accuracy of the sampling is low. The atoms are moved along their own x, y, z directions for a step that does not depend on the nature of the single chemical

species. The accuracy in the evaluation of the numerical second derivatives is improved by choosing a proper atomic displacement to sample the PES. A first improvement would be the use of mass-weighted coordinates in order to adapt the step regarding each single atomic mass. However, this procedure still does not improve substantially the accuracy of the frequencies. The most appropriate choice is again a transformation from Cartesian to normal mode displacements in order to sample directly energy and gradients along the coordinates in which the oscillations take place. Using the **S** transformation matrix of eq. 2.12, Cartesian displacements can be performed along each normal mode independently. Similarly to eq. 2.15, the equilibrium structure $\mathbf{x}_0$ can be distorted along each normal mode individually in the positive or negative direction

$$\mathbf{x}_k^{disp} = \mathbf{x}_0 \pm P\,dQ_k^{disp}\mathbf{v}_k. \tag{2.16}$$

The integer P runs from 1 to n_{grid} that is the number of symmetric grid points used to sample the PES, dQ_k^{disp} is the magnitude of the displacement defined as $dQ_k^{disp} = 4/\sqrt{2\pi\omega_k}2n_{grid}$, $\mathbf{v}_k$ is the eigenvector of the k-th mode and $\mathbf{x}_0$ is the equilibrium structure. This displacement entity corresponds to the classical turning points of an harmonic oscillator with a frequency ω_k. From the quantum mechanics point of view, this ensures that the wave function decays to zero at these points.

Since in the basis of normal mode coordinates the Hessian matrix is diagonal by construction each single eigenvalue, i.e. frequency, can be evaluated individually by numerical second order differentiation of the energy. Considering for example the two first positive and negative displacements corresponding to $P = 1, -1$, the k-th Hessian diagonal element is calculated as

$$F_{kk} = \frac{E_{-1} + E_1}{(dQ_k^{disp})^2} \tag{2.17}$$

where the central value $E(0)$ is referenced as zero of the energy. These diagonal elements of the Hessian matrix **F** are related to the vibrational frequencies through $\nu_k = \omega_k/2\pi = \sqrt{F_{kk}}/2\pi$. Expression 2.17 can be easily extended to more than 2 points following the scheme proposed by Fornberg [104] as summarized in Table 2.1.

In a similar fashion, the diagonal elements of the Hessian matrix **F** can be

Table 2.1: *Second order central difference formulas.*

$2n_{grid}$	Second Order Formula
2	$\frac{E_{-1} + E_1}{(dQ_k^{disp})^2}$
4	$\frac{-E_{-2} + 16E_{-1} + 16E_1 - E_2}{12(dQ_k^{disp})^2}$
6	$\frac{2E_{-3} - 27E_{-2} + 270E_{-1} + 270E_1 - 27E_2 + 2E_3}{180(dQ_k^{disp})^2}$
8	$\frac{-9E_{-4} + 128E_{-3} - 1008E_{-2} + 8064E_{-1} + 8064E_1 - 1008E_2 + 128E_3 + 9E_4}{5040(dQ_k^{disp})^2}$

Table 2.2: *First order central difference formulas.*

$2n_{grid}$	First Order Formula[a]
2	$\frac{-g_{-1} + g_1}{2dQ_k^{disp}}$
4	$\frac{g_{-2} - 8g_{-1} + 8g_1 - g_2}{12dQ_k^{disp}}$
6	$\frac{-g_{-3} + 9g_{-2} - 45g_{-1} + 45g_1 - 9g_2 + g_3}{60dQ_k^{disp}}$
8	$\frac{3g_{-4} - 32g_{-3} + 168g_{-2} - 672g_{-1} + 672g_1 - 168g_2 + 32g_3 - 3g_4}{840dQ_k^{disp}}$

[a] Here g_P stands for the k-th element of the normal mode gradient vector calculated from the Cartesian gradient as $\mathbf{g_Q} = \mathbf{S}^T\mathbf{g_x}$.

calculated numerically starting from the normal mode gradients $\mathbf{g_Q}$ using first order formulas (see Table 2.2).

Calculating harmonic frequencies along the normal modes allows the calculation of several points on the PES ensuring that the distortions take place in the proper direction enhancing the accuracy of the sampling.

Moreover, at the same time, if the procedure maps enough points on the PES, this can be fit to a polynomial of a given order and used to calculate anharmonic corrections to the frequencies as described in the next section.

2.7 Quantum Diagonal Anharmonicity

Correcting the harmonic frequencies of a chemical system for anharmonic effects is an important step in the study of molecular and crystal vibrations. This is not only important for the accurate prediction of spectroscopical properties such as IR, Raman or photoelectron spectroscopy, but also to calculate thermodynamic functions within chemical accuracy [26]. Many methods and theories of varying accuracy have been proposed to reach this goal. The correction schemes proposed go from simple semi-empirical scaling of the calculated frequencies [105] to exact solutions of model potentials such as the Morse potential [106], perturbation theory [107], variational method [24] up to very sophisticated methods such as vibrational self-consistent field (VSCF) [108–110].

In this work, anharmonicity has been treated variationally using a model potential derived by fitting the PES along each normal mode independently, i.e. neglecting mode-mode coupling. The aim is to solve the Schrödinger equation variationally for all the normal modes independently in a basis of harmonic functions with a sixth order model potential. The Hamiltonian for a generic k-th mode is

$$H = -\frac{\hbar^2}{2}\frac{d^2}{dQ_k^2} + a_0 + a_1 Q_k + a_2 Q_k^2 + a_3 Q_k^3 + a_4 Q_k^4 + a_5 Q_k^5 + a_6 Q_k^6 \tag{2.18}$$

with Q_k being the normal coordinate of the mode and a_i ($i = 0, \ldots, 6$) the polynomial fitting coefficients of the potential. The Hamiltonian matrix elements

$$H_{mn} = \langle \phi_m | H | \phi_n \rangle \tag{2.19}$$

are defined with the harmonic functions ϕ_m which are solutions of the

one dimensional quantum harmonic oscillator

$$\phi_m = \sqrt{\frac{1}{2^m m!}} \left(\frac{\omega_k}{\pi\hbar}\right)^{\frac{1}{4}} e^{-\frac{\omega_k}{2\hbar} Q_k^2} \mathcal{H}_m \left(\sqrt{\frac{\omega_k}{\hbar}} Q_k^2\right) \tag{2.20}$$

with $m = 0, 1, \ldots$ and $\mathcal{H}_m$ being the $m-$th order Hermite Polynomial. After application of Hermite polynomial rules to eq. 2.19, the matrix elements can be derived analytically as reported in Table 2.3.

Table 2.3: *Anharmonic hamiltonian matrix elements.*

H_{mn}	Integral value[a]
δ_{mn}	$-\frac{1}{2}U(2m+1) + a_0 + \frac{1}{2}a_2V^2(2m+1) +$ $\frac{1}{4}a_4V^4(6m^2+6m+3) + \frac{1}{8}a_6V^6(20m^3+30m^2+40m+15)$
$\delta_{m(n+1)}$	$\sqrt{2m}\left[\frac{1}{2}a_1V + \frac{1}{4}a_3V^3m + \frac{1}{8}a_5V^5(10m^2+5)\right]$
$\delta_{m(n+2)}$	$\sqrt{m(m-1)}\left[\frac{1}{2}U + \frac{1}{2}a_2V^2 + \frac{1}{4}a_4V^4(4m-2) + \frac{15}{8}a_6V^6(m^2-m+1)\right]$
$\delta_{m(n+3)}$	$\sqrt{m(m-1)(m-2)}\left[\frac{1}{\sqrt{8}}a_3V^3 + \frac{\sqrt{2}}{8}a_5V^5(5m-5)\right]$
$\delta_{m(n+4)}$	$\sqrt{m(m-1)(m-2)(m-3)}\left[\frac{1}{4}a_4V^4 + \frac{1}{8}a_6V^6(6m-9)\right]$
$\delta_{m(n+5)}$	$\sqrt{\frac{1}{32}}\sqrt{m(m-1)(m-2)(m-3)(m-4)}a_5V^5$
$\delta_{m(n+6)}$	$\frac{1}{8}\sqrt{m(m-1)(m-2)(m-3)(m-4)(m-5)}a_6V^6$

[a] where $U = -\frac{\hbar\omega_k}{2}$ and $V = \sqrt{\frac{\hbar}{\omega_k}}$.

Diagonalization of the Hamiltonian matrix for a certain number of harmonic basis functions yields the eigenvalues ϵ_i of the energy states of

the anharmonic oscillator. The quantum anharmonic vibrational partition function is approximated as a truncated sum over the states

$$q_a = \sum_{i=0}^{\infty} e^{\frac{\epsilon_i}{k_B T}} \approx \sum_{i=0}^{m} e^{\frac{\epsilon_i}{k_B T}}. \tag{2.21}$$

Its convergence with respect to the number of states, given by the number of harmonic oscillator functions ($\Delta q_a = q_a^m - q_a^{m-1} < \sigma$, where σ is a reasonably small number), is used as variational criterion. This condition is combined with the convergence of the fundamental anharmonic frequency of the oscillator $\Delta \nu_a = \nu_a^m - \nu_a^{m-1} < \delta$, where $\nu_a = (\epsilon_1 - \epsilon_0)/h$ (h here is the Planck's constant). When converged, the energy states are used to calculate internal energies and entropies.

In order to obtain anharmonic vibrational internal energies and entropies from the sum over the states partition function in (N, V, T) conditions, the sum over the states formulas are plugged into the expressions relating the partition function to the thermodynamical functions

$$E_{v,a} = N k_B T^2 \frac{\partial \ln q_a}{\partial T} \tag{2.22}$$

$$S_{v,a} = N k_B \ln q + N k_B T \frac{\partial \ln q_a}{\partial T} \tag{2.23}$$

yielding the following equations for internal energy and entropy:

$$E_{v,a} = N \frac{\sum_{i=0}^{m} \epsilon_i e^{\frac{\epsilon_i}{k_B T}}}{\sum_{i=0}^{m} e^{\frac{\epsilon_i}{k_B T}}} \tag{2.24}$$

$$S_{v,a} = N k_B \ln \left(\sum_{i=0}^{m} e^{\frac{\epsilon_i}{k_B T}} \right) + \frac{N}{T} \frac{\sum_{i=0}^{m} \epsilon_i e^{\frac{\epsilon_i}{k_B T}}}{\sum_{i=0}^{m} e^{\frac{\epsilon_i}{k_B T}}} \tag{2.25}$$

2.8 Proper Sampling of the Potential Energy Surface

At first sight, sampling the PES according to eq. 2.16 looks straightforward. The structure is displaced along the normal mode coordinates and each point on the grid corresponds to a specific energy on the PES. The question that must be addressed is: how good is this sampling? One a problem is that normal mode distortions in Cartesian coordinates are rectilinear by definition. Therefore, they do not preserve any internal coordinate, it is not possible to change, e.g. a bond angle, without changing also a bond distance. Thus the diagonal potential does not directly correspond to a stretch, bend or torsion, but rather to a mixture of all these internal coordinates. Furthermore, normal mode rectilinear distortions are valid for infinitesimal displacements only. This means that any finite displacement, albeit very small, could always be too large to respect the validity of the linear relation. Moreover, the energy itself is calculated using numerical methods. Therefore, there is a limit on the precision that can be achieved. This fact imposes the use a sufficiently large displacement able to produce a reasonable energy change that makes negligible the effect of the numerical noise. This two counterparts are clearly in opposition. Too large steps distort the structure without preserving the internal coordinates but too small steps do not allow a numerically stable energy sampling. Figure 2.1 shows a schematic representation of an angle bending mode of a generic triatomic molecule. It can be observed that using finite (not infinitesimal) linear displacements the two terminal atoms follow a line path. The consequence of this is that the bond distance between the two terminal atoms and the central one elongates when varying the angle. In the case of curvilinear displacements the terminal atoms follow a circular line. This means that when the angle is changed the two terminal atoms are kept at a fixed distance form the central atoms.

For high frequency vibrations which have low vibrational amplitudes, linear (Cartesian) displacements are still a good approximation for a correct sampling of the PES. However, for low frequency/high amplitude vibrations, linear displacements result in an artificial coupling of all vibrations. Therefore, the sampling does not catch the correct shape of the PES. Since stretching modes are linear by construction, they are in general not affected by such problems whereas bends and torsion are lin-

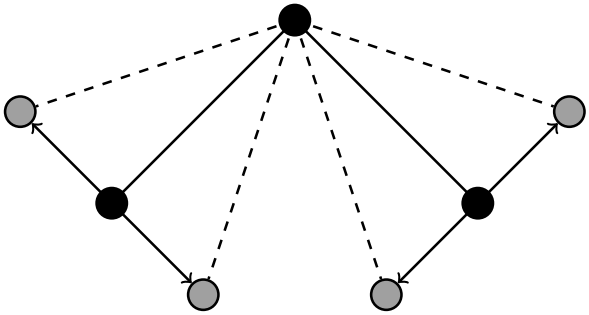

(a) *linear*

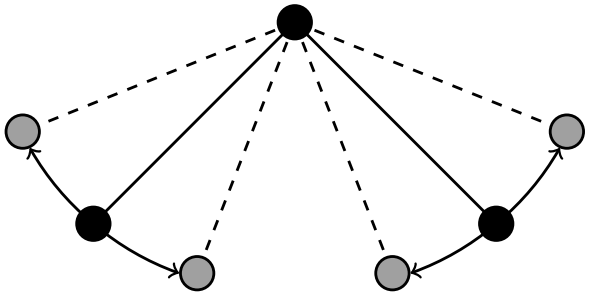

(b) *curvilinear*

Figure 2.1: *Schematic representation of an angle bend normal mode motion showing the results of linear Cartesian displacements (a) and curvilinear internal ones (b).*

ear for infinitesimal displacements only [92, 111]. In describing low frequency/high amplitude motions, e.g. in weakly bound systems [28, 29], rectilinear normal mode displacements (linear combinations of Cartesian coordinates) are not sufficient. Njegic and Gordon suggested to improve the sampling of the PES by employing curvilinear normal mode displacements defined using internal coordinates. They have shown [26] that this approach has a strong effect on the thermodynamics of formation of some simple molecular systems. Here follows the theoretical background of the

transformation of normal modes using internal coordinates and the way to improve the sampling of the PES.

In this work, the sampling scheme in curvilinear normal mode displacements is adapted to treat quantum diagonal anharmonicity in extended systems in order to get entropy estimates with chemical accuracy. The definition of internal coordinates for periodic systems, i.e. including periodic images in the definition of the topology, has been discussed in different works [112–114]. The present work uses the definition of periodic redundant internal coordinates proposed by Bučko et al. [114] due to its completeness in defining intra and inter cell bonds and follows Boatz and Gordon [25] in defining a Wilson transformation of the normal modes in internal coordinates. The well known B-matrix [92] gives the relationship between Cartesian displacement coordinates and internal coordinates,

$$\boldsymbol{\Delta R} = \mathbf{B}\boldsymbol{\Delta x}, \quad \text{where} \quad B_{i,j} = \frac{\partial R_i}{\partial x_j} \tag{2.26}$$

Simple internal coordinates are defined as stretching, bends and torsions and the dimension of their space can vary from $3N-6$, $3N-5$ or $3N-3$ for a non-linear, linear and periodic system, respectively (non-redundant set) up to a specific number S (redundant set). The use of the latter set is critical for a proper description of the vibrational modes as also suggested by Boatz and Gordon [25] and others [115–120]. Independently of the choice of the internal coordinates, the Cartesian Hessian matrix can be transformed into internals as

$$\boldsymbol{\Phi} = (\mathbf{B}^{-1})^{\mathsf{T}}\mathbf{H}(\mathbf{B}^{-1}) \text{ and vice versa } \mathbf{H} = \mathbf{B}^{\mathsf{T}}\boldsymbol{\Phi}\mathbf{B} \tag{2.27}$$

where $\boldsymbol{\Phi}$ is the Hessian matrix in internal coordinates. From the definition of the diagonal Hessian of eqs. 2.10 and 2.12

$$\mathbf{S}^{\mathsf{T}}\mathbf{H}\mathbf{S} = \mathbf{F}, \text{ where } \mathbf{S} = \mathbf{M}^{-\frac{1}{2}}\mathbf{s} \tag{2.28}$$

and substituting the Cartesian Hessian (eq. 2.27) it follows that

$$\mathbf{F} = \mathbf{S}^{\mathsf{T}}(\mathbf{B}^{\mathsf{T}}\boldsymbol{\Phi}\mathbf{B})\mathbf{S} = \mathbf{D}^{\mathsf{T}}\boldsymbol{\Phi}\mathbf{D} \tag{2.29}$$

where the matrix

$$\mathbf{D} = \mathbf{BS} \tag{2.30}$$

is the matrix of normal mode eigenvectors $[\gamma_1, \gamma_2, \cdots, \gamma_{3N}]$. Each column corresponds to the internal coordinates coefficients of the linear combination for a generic k-th normal mode. Having these eigenvectors, the Cartesian equilibrium geometry can be distorted along each normal mode by a displacement $\sigma_k = PdQ_k^{disp}\gamma_k$

$$\mathbf{x}_k^{disp} = \mathbf{x}_0 \pm (\mathbf{B}^{-1})^T \sigma_k \tag{2.31}$$

Since by construction internal coordinates are non linear (curvilinear), the above equation must be solved iteratively as well documented in the literature [111, 121–123]. From the new Cartesian coordinates of eq. 2.31, a new set of internal coordinates is calculated as $\Delta\mathbf{R}_n = \sigma_k - (\mathbf{R}_n - \mathbf{R}_0)$ where n is the iteration counter. The quantity $\Delta\mathbf{R}_n$ represents the difference between the desired displacement in internal coordinates σ_k and the actual one during the iterative back-transformation. The latter is then used to calculate a new Cartesian geometry $\mathbf{x}_{k,n+1}^{disp} = \mathbf{x}_{k,n}^{disp} + (\mathbf{B}^{-1})^T\Delta\mathbf{R}_n$. The iteration is looped until $(\mathbf{B}^{-1})^T\Delta\mathbf{R}_n < 10^{-6}$ or $n > 25$. In some cases, the iteration might diverge during the refinement, therefore, if $\Delta\mathbf{R}_n > \Delta\mathbf{R}_1$, the procedure is stopped and Cartesian geometry is reverted to the first estimate $\mathbf{x}_1^{disp}$. While in general such a procedure is acceptable in structure optimizations, it might be source of severe accuracy problems when trying to sample the PES. A proper choice of the internal coordinates has proven to be essential to ensure convergence of the transformation.

A last remark must be spent on the definition of the inverse of the B-matrix. Since in general the B-matrix is rectangular, no direct inverse matrix can be calculated. To calculate the inverse, several methods have been proposed [25, 123, 124]. The derivation employed in this work follows the indications of Boatz and Gordon [25] and Pulay and Fogarasi [124]. The goal is to remove the redundancies of $\mathbf{B}$ which are the linearly dependent rows of the matrix. A squared $\mathbf{G}$ matrix (also know as the Wilson G-matrix) is defined as

$$\mathbf{G} = \mathbf{BM}^{-1}\mathbf{B}^T \tag{2.32}$$

where $\mathbf{M}^{-1}$ is the inverse of the atomic mass matrix defined above. The eigenvalue equation of $\mathbf{G}$

$$\mathbf{G}\begin{pmatrix} \mathbf{K} & \mathbf{L} \end{pmatrix} = \begin{pmatrix} \mathbf{K} & \mathbf{L} \end{pmatrix} \begin{pmatrix} \mathbf{\Lambda} & \mathbf{0} \\ \mathbf{0} & \mathbf{0} \end{pmatrix} \tag{2.33}$$

has $3N - m$ ($m = 6, 5, 3$) *nonzero* eigenvalues and $S - (3N - m)$ zero eigenvalues corresponding to the redundancies therefore the matrix is singular and cannot be inverted directly. The generalized inverse of the matrix $\mathbf{G}$ is obtained from eq. 2.33 as

$$\mathbf{G}^{-1} = \begin{pmatrix} \mathbf{K} & \mathbf{L} \end{pmatrix} \begin{pmatrix} \mathbf{\Lambda}^{-1} & \mathbf{0} \\ \mathbf{0} & \mathbf{0} \end{pmatrix} \begin{pmatrix} \mathbf{K}^{T} \\ \mathbf{L}^{T} \end{pmatrix} \tag{2.34}$$

transforming it to diagonal form and inverting only the *nonzero* eigenvalues. Therefore taking the inverse of both sides of eq. 2.32

$$\begin{aligned} \mathbf{G}^{-1} &= \left(\mathbf{B}\mathbf{M}^{-1}\mathbf{B}^{T}\right)^{-1} \\ \mathbf{G}^{-1} &= \left(\mathbf{B}^{-1}\right)^{T}\mathbf{M}\mathbf{B}^{-1} \end{aligned} \tag{2.35}$$

the expression for the generalized inverse of the B-matrix is obtained

$$\mathbf{B}^{-1} = \mathbf{M}^{-1}\mathbf{B}^{T}\mathbf{G}^{-1} \tag{2.36}$$

When treating large systems with many redundancies, the calculation and subsequent inversion of $\mathbf{G}$ can be computationally demanding. Having this expression for the inverse B-matrix, it can be used in the procedure for the internal to Cartesian coordinates back-iteration.

2.9 Hybrid MP2:DFT Optimization

In computational molecular and material sciences Kohn-Sham density functional theory DFT [4, 125–128] is widely used. Its success is motivated by the fact that calculations are possible of a wide range of chemical systems on a relatively large scale with an appreciable accuracy of the results. Since the exact exchange and correlation density functional is unknown, many approximations of higher accuracy in describing the system have been proposed. The hierarchy of exchange and correlation density functional is divided into different types of approximations going from local

density approximation (LDA) to generalized gradient approximation that incorporates first (GGA) or higher (meta-GGA) derivatives of the electron density. Even higher improvement is achieved when including a fraction of the exact Fock exchange such as in hybrid functionals (e.g. BLYP [129] functionals family). Experience shows that the latter yields reliable results for many chemical systems. However, the treatment of large periodic systems (such as solid catalysts) makes these calculations extremely expensive. Unfortunately, pure GGA type functionals, that are computationally more efficient in particular with plane waves, are not accurate enough, especially in the description of the adsorption complexes (long-range correlation, i.e. dispersion) or in the estimation of reaction barriers (self interaction error). A partial solution of the first problem is adding a semi-empirical dispersion term as proposed by Grimme [130]. However, despite a substantial improvement, the desired chemical accuracy limit ($\pm$ 1 kcal/mol $\approx \pm$ 4.2 kJ/mol) is not reached.

To include both long range correlation effects for a better description of the dispersion and Hartree-Fock exchange to avoid the self interaction error, a hybrid high-level quantum mechanics - low level quantum mechanics mechanical embedding scheme [131, 132] is used. It combines second-order Møller-Plesset perturbation theory (MP2) [133–136] for a cluster model of the adsorption complex as the high level method with density functional theory [18, 125] for the full periodic structure of the adsorbed molecule - surface (active site) system. The hybrid QM:QM energy is defined within a subtractive scheme [137]:

$$\begin{aligned} E_{HL:LL}(pbc) &= E_{LL}(pbc) - E_{LL}(C) + E_{HL}(C) \\ &= E_{HL}(C) + \Delta_{LR}(pbc, C) \\ &= E_{LL}(pbc) + \Delta_{HL}(C) \end{aligned} \tag{2.37}$$

where $E_{LL}(pbc)$ is the low level energy of the adsorbed molecule - surface system including periodic boundary conditions, $E_{LL}(C)$ is the low level energy for the cluster model of the adsorbed molecule on the surface, and $E_{HL}(C)$ is the high level energy for the same finite size cluster models. The result can be viewed as a high level calculation for the cluster model, $E_{HL}(C)$, to which a long-range correction,

$$\Delta_{LR}(pbc, C) = E_{LL}(pbc) - E_{LL}(C) \tag{2.38}$$

evaluated at the low level, has been added, or a low level calculation with periodic boundary conditions for the full structure, to which a high level correction,

$$\Delta_{HL}(C) = E_{HL}(C) - E_{LL}(C) \tag{2.39}$$

evaluated for the cluster model, has been added. The dangling bonds of the cut-out defining the high level cluster are terminated with hydrogen "link" atoms [137]. Structure optimizations are performed on the combined potential energy surface defined by eq. 2.37 with forces calculated by the same subtraction scheme [137, 138],

$$f_{i,HL:LL}(pbc) = f_{i,LL}(pbc) - f_{i,LL}(C) + f_{i,HL}(C) \tag{2.40}$$

For a given (high level) QM method, the results are affected by the incompleteness of atom-centered basis sets, resulting in the Basis Set Superposition Error (BSSE) [139] and the Basis Set Incompleteness Error (BSIE) [140]. Substantial improvements with respect to the complete basis set (CBS) limit can be achieved if an extrapolation is performed on the BSSE-free potential energy surface [141]. The adopted procedure, CPC-CBS scheme, allows us to unmask the Basis Set Incompleteness Error (BSIE) and to investigate Basis Set Superposition Error (BSSE)-free PES. For the interaction of a molecule A with a surface S, the binding energy is defined as

$$\Delta E = E_{A-S} - E_A - E_S \tag{2.41}$$

The unphysical lowering of the energy of the complex due to the presence of the basis function of the other sub-system, ϵ, according to the function counterpoise scheme of Boys and Bernardi [139], is:

$$\epsilon = [E(A//A-S) - E(\{S\}A//A-S)] + [E(S//A-S) - E(S\{A\}//A-S)] \tag{2.42}$$

where $A//A-S$ and $S//A-S$ are the two components in their frozen complex structure. In particular, $E(\{S\}A)$ and $E(S\{A\})$ are the energies of the components A and S, respectively, in presence of the total basis set of the complex $A-S$. Counterpoise-corrected binding energies are obtained

as

$$\Delta E_{cpc} = \Delta E + \epsilon \tag{2.43}$$

The extrapolation of the CPC-energies uses Dunnings correlation consistent basis sets for two consecutive cardinal numbers X=2 (double-ζ, D) and X=3 (triple-ζ, T) in the present case [140]. For the Hartree-Fock (HF) part, an exponential extrapolation scheme is applied [142, 143]

$$E_{HF,X} = E_{HF,\infty} + A \exp(-1.5X) \tag{2.44}$$

while an inverse power law is used for the correlation energy [144]

$$E_{corr,X} = E_{corr,\infty} + AX^{-3}. \tag{2.45}$$

This defines a multi-level computational scheme that combines the subtraction scheme for embedded cluster calculations, eqs. 2.37 and 2.40, with basis set extrapolation for the counterpoise corrected high-level (here MP2) cluster energy. This multilevel method avoids artifacts in the equilibrium structure prediction as for example a typically too short distance between the adsorbed molecule and the surface.

2.10 Computational Protocol

Figure 2.2 shows a flowchart of the protocol applied in this work to obtain accurate estimates of thermodynamic functions of adsorption. The programs employed to calculate specific quantities, namely structures, energies, and vibrational frequencies, are highlighted in blue.

2.11 Models and Computational Details

In this section, the structural models employed in the periodic and cluster calculations for the system studied in this work are reported with the respective computational details.

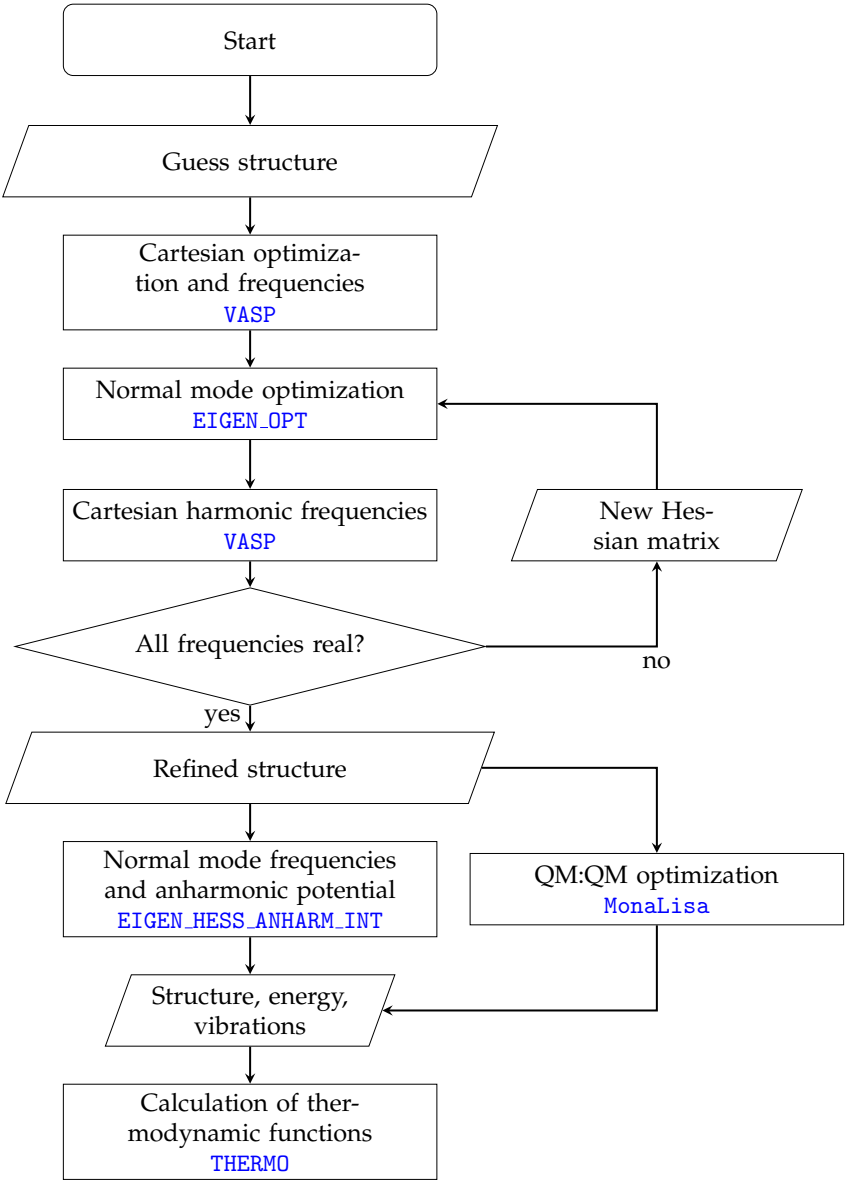

Figure 2.2: *Flowchart of the computational protocol described and used in this work. In capital blue letter the computer programs used at each specific step are reported.*

2.11.1 Calculations with Periodic Boundary Conditions

Methane on MgO(001)

To model the adsorption of methane on the MgO(001) surface, the "ROT" structure [39] has been adopted which was also considered by Tosoni and Sauer [44] (cf. Figure 2.3). It consists of a slab of three layers of magnesium oxide where at each surface four methane molecules are adsorbed. The surface is a $2a \times 2a$ supercell formed by three layers of MgO. The 2×2 double cell is mandatory to accommodate the methane molecules in this particular arrangement. The dimensions of the orthorhombic unit cell are $8.42 \times 8.42 \times 25.00$ Å. The size of the c lattice parameter ensures enough vacuum to avoid artificial interactions between the periodic images.

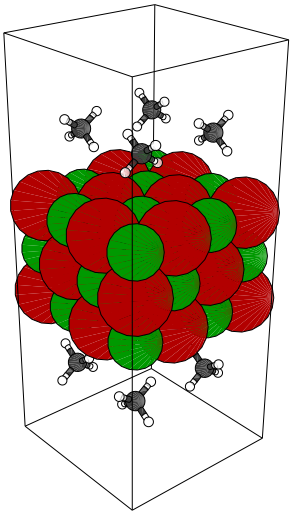

Figure 2.3: *Slab model for methane adsorption on MgO(100) surface proposed by Tosoni and Sauer [44] showing the double monolayer structure on each side of the slab. Color key: green - megnesium, red - oxygen, gray - carbon, and white - hydrogen.*

The gas phase calculation of the methane molecule has been performed for an orthorhombic supercell of $8.42 \times 8.42 \times 25.00$ Å.

A 400 eV energy cutoff has been been employed using projector-aug-

mented wave (PAW) scheme [145, 146]. The threshold for energy convergence between two consecutive SCF cycles is 10^{-8} eV/cell. The reciprocal space has been sampled using a Monkhorst-Pack grid [147] of 2×2×1 k-points. To describe properly the dispersion interactions for Mg^{2+} ions, the Grimme's parameters for Ne have been used ($c_6 = 0.63$ and $R_6 = 1.243$) as proposed in ref. [44], combined with the PBE [148] functional. The Hessian matrix has been calculated for each structure using VASP Cartesian central displacements providing the initial guess for the eigenvectors to be used in the normal mode optimization. Optimization in normal mode coordinates was implemented in the program EIGEN_OPT [1] and applied to each structure. Since the sampling of the energy is more accurate using normal mode coordinates, it has been possible to converge the gradients up to 10^{-6} eV/Å. Calculation of harmonic frequencies in normal mode coordinates and fit of the PES to a sixth order polynomial was implemented in the program EIGEN_HESS_ANHARM_INT [2]. Both programs are written in Fortran90 (F90) and interfaced with VASP [18] in order to get total energies and gradients from single point calculations and Hessian matrix to get frequencies and corresponding eigenvectors. The calculation of the internal coordinates and relative B-matrix are performed using the Python script WriteBmatrix.py by Tomas Bučko [114].

Methane, Ethane, and Propane in H-CHA

Figure 2.4 shows the model H-CHA (or H-SSZ-13) supercell employed in the periodic calculations. The structure of interest is a 2a monoclinic supercell of acidic chabazite ($a = 18.90$ Å, $b = 9.44$ Å, $c = 9.29$, $\alpha = 94.0°$, $\beta = 94.9°$, $\gamma = 95.4°$). The supercell accommodates two substitutional Al atoms, i.e. two active sites. The total Si/Al ratio is 11/1. The acidic hydrogen is located at the O2 position following the work of Bučko [30].

Although the unit cell of chabazite is trigonal ($R\bar{3}m$, $a = 9.4$ Å, $\alpha = 94°$ [80]), the monoclinic model employed allows a low Si/Al ratio and ensures a negligible lateral interaction between the adsorbed molecules. This model has been largely employed in many computational works [6, 30–32, 149]. Each of the adsorbed molecule forms a complex with only one of the two Brønsted acidic sites present in the supercell. Methane, ethane and propane molecules have been put in a cubic cell of 15×15×15 Å. This avoids fictitious later interaction between period images for the gas phase molecules.

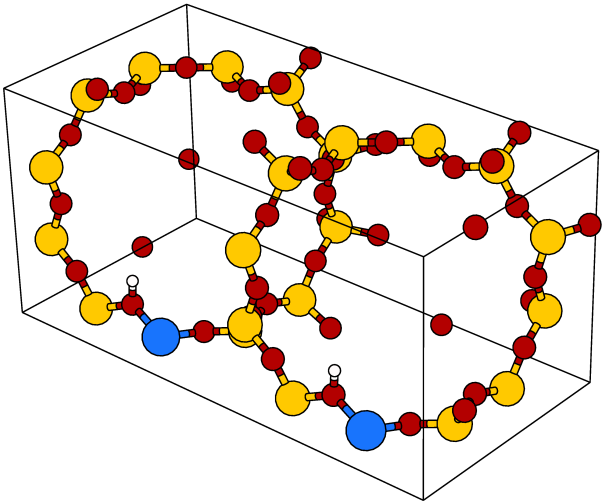

Figure 2.4: *H-CHA* 2a *supercell showing the acidic hydrogens in position O2 (oxygen shared by 2 8-membered ring and 1 4-membered rings). Color key: yellow - silicon, red - oxygen, blue - aluminum, and white - hydrogen.*

Each plane-wave calculation has been performed using the VASP program [18]. A 600 eV energy cutoff at the Γ-point only has been employed using the projector-augmented wave (PAW) scheme [145, 146]. The threshold for energy convergence between two consecutive SCF cycles is 10^{-8} eV/cell. The PBE [148] functional has been employed using Grimme's "D2" parameters [130] to include dispersion interactions [150]. All the structures have been pre-optimized using VASP conjugate gradients algorithm converging the gradients up to 10^{-4} eV/Å. Optimization in normal mode coordinates and frequency calculation have been carried out using the same approach described for the case of alkanes adsorption on the MgO(001) surface.

2.11.2 Cluster Calculations

Methane, Ethane and Propane in H-CHA

The clusters employed in the low and high level calculations are $8\,T_{11H}$ (following the nomenclature of refs. [7, 131, 132]) as shown in Figure 2.5 where each Si, O and Al dangling bond has been passivated with a terminal H atom along the direction of the broken bond. The structures are cut out of the normal mode optimized periodic structures. The criterion used for selecting the atoms of the cluster is based on a sphere of 500 pm radius around the adsorbed carbon atom of the alkane. Based on this rule, every cluster resulted to be isostructural to each other. The same geometry has been used for the free H-CHA cluster (see Figure 2.5).

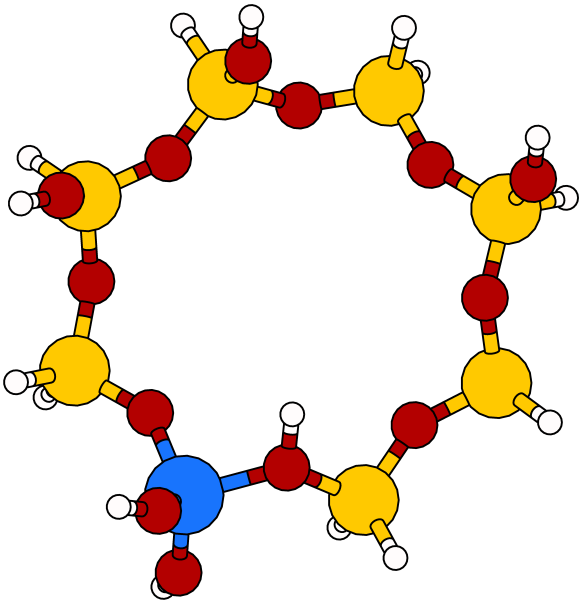

Figure 2.5: *$8\,T_{11H}$ cluster model employed in the hybrid MP2:DFT+D calculations. Color key: yellow - silicon, red - oxygen, blue - aluminum, and white - hydrogen.*

For the high level part of the hybrid scheme, MP2 calculations have been carried out using the resolution of identity (RI)-CC2 module [133,

135, 136] available in version 6.5 of the TURBOMOLE program [134]. For all atoms in the system, Dunning's correlation-consistent polarized valence basis sets (cc-pVXZ) of systematic increasing quality from X=2 (double-ζ, D) to X=3 (double-ζ, T) [140, 151] have been used and 1*s* frozen-core approximation applied. For the low level, part the clusters have been put in a cubic cell of $20\times20\times20$ Åto avoid interactions with the periodic images. The settings of the calculations are identical to the ones used to calculate the periodic structures for alkanes in H-CHA.

3 Results and Discussion

3.1 Normal Mode Coordinate Optimization

3.1.1 Methane, Ethane, and Propane

First, the three small molecules of interest for the adsorption studies have been considered. Structural optimization in normal mode coordinates leads to lower energy structures (see Figure 3.1).

It is no surprise that for methane and ethane the effect of structure refinement is rather small in the energy whereas for propane the change is noticeable ($\sim$ 0.19 kJ/mol). It mainly arises from the optimization of different hindered rotor modes which, due to the flatness of the potential energy surface, cannot be accurately minimized using common coordinates. While the energy minimization converges after very few steps, the gradients (considered in this study as the only criterion to stop the minimization process) need more steps. This feature can be ascribed to two possible opposite driving forces. While the gradient is a vector quantity and contains much more detailed information, it suffers, for the same reason, from more numerical noise. On the other hand the energy is a scalar with averaged information. Therefore, the noise is more systematic resulting in a faster convergence of this parameter during the optimization.

3.1.2 Adsorption Structures in H-chabazite

The accurate determination of the adsorption structures of molecules at a catalytic site is a challenging goal in the field of theoretical catalysis. One of the main structural features of zeolites is the floppiness of their lattices. This makes zeolites very susceptible to external perturbations such as molecules entering the cavity. Therefore, the optimization of such structures, involving floppy motions of the zeolite framework and low frequency motions (*hindered* translations and rotations relative to the framework) of the adsorbed molecules [14], can be not trivial.

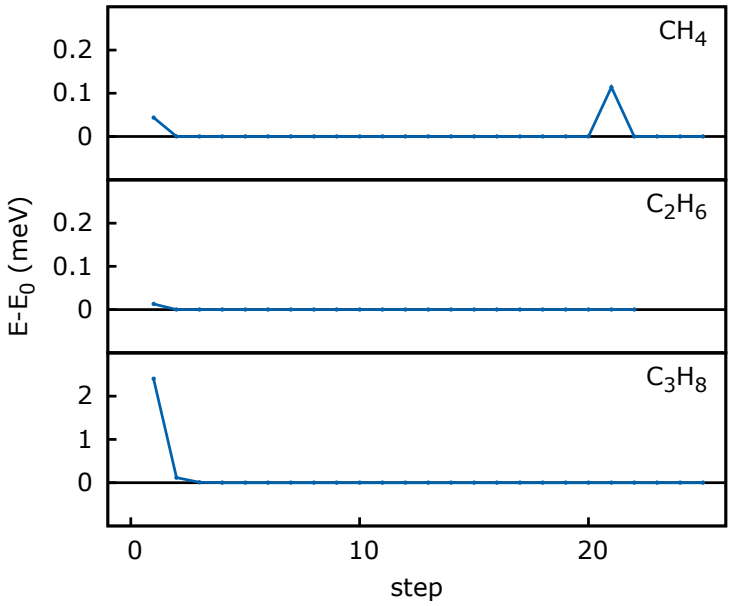

Figure 3.1: *Energy minimization profile for methane, ethane and propane under normal mode coordinates optimization.*

Once a reference structure has been pre-optimized using standard cartesian optimization methods, a more accurate minimization can be applied in order to refine the structure. In Figure 3.2, the energy minimization profiles for the adsorption structures of methane, ethane and propane at the catalytic OH group are reported.

The effect of the optimization in normal coordinates on the energy is much more evident. While for unloaded H-CHA and for the methane adsorption complex the optimization leads to a simple structural relaxation, with the energy smoothly converging, in the other cases a local rearrangement is taking place. The "bumps" in the profiles at the beginning of the minimizations indicate substantial structural changes. This fact shows that the optimization scheme, exploring the local PES, is able

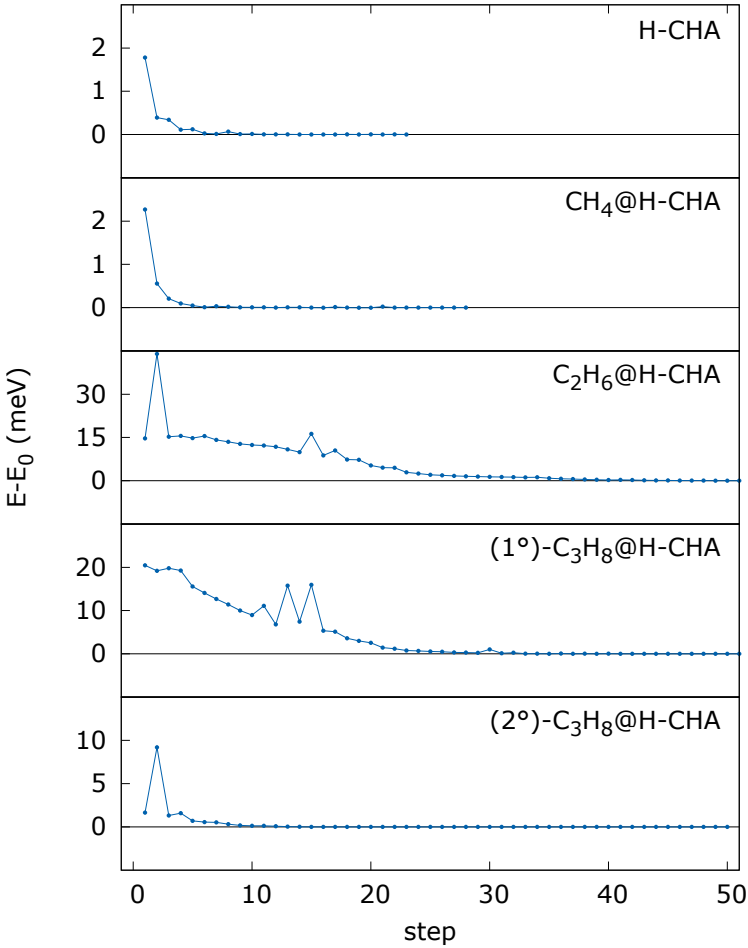

Figure 3.2: *Energy minimization profile for structure refinement using optimization in normal mode coordinates. Unloaded H-CHA and its adsorption complexes with methane, ethane, and propane adsorbed via primary and secondary carbon.*

to find more stable configurations. This is not surprising since the implemented algorithm uses the RFO approach [97] to calculate the steps allowing the search for other stationary points in the neighboring region and supplying a better description of the local PES through a [2/2] Padé approximant. This is a major improvement in such anharmonic regions.

Figure 3.3 shows the adsorption complexes. As a common structural motif, the acidic hydrogen in O2 position points toward the carbon atom, extending its coordination sphere by a fifth hydrogen atom, however at much larger distance. Table 3.1 reports the most relevant interatomic distances (r_1 ($r_{C\cdots H(O)}$), r_2 ($r_{(C)H\cdots O}$)). Using the method proposed here, the local coordination of the alkane does not change much depending on the carbon number. This is expected since the methyl and ethyl groups of adsorbed ethane and propane are not involved in the specific interaction of the methyl group with the surface OH group. This feature was not observed in previous calculations using standard optimization techniques with Cartesian coordinates [6, 30].

Table 3.1: *Relevant bond distances (pm) for adsorption complexes.*

Alkane	PBE+D (this work)		PBE+D [6]	PW91 [30]	
	r_1	r_2	r_1	r_1	r_2
methane	215	256	212	247	364
ethane	214	273	236	235	252
propane(C(1°))[a]	213	264	238	240	252
propane(C(2°))[b]	218	264	–	251	255

[a] Propane adsorbed via primary carbon to hydroxyl group.
[b] Propane adsorbed via secondary carbon to hydroxyl group.

Comparison of the electronic adsorption energies (Table 3.2) shows a rather small but general stabilization of the adsorption complexes whose structures have been refined by re-optimization in normal coordinates. If the absolute energies are taken into account, it is clear that the structural changes are extremely relevant. It will be shown below how the frequencies and thus the vibrational energies are affected by changes of the reference structures.

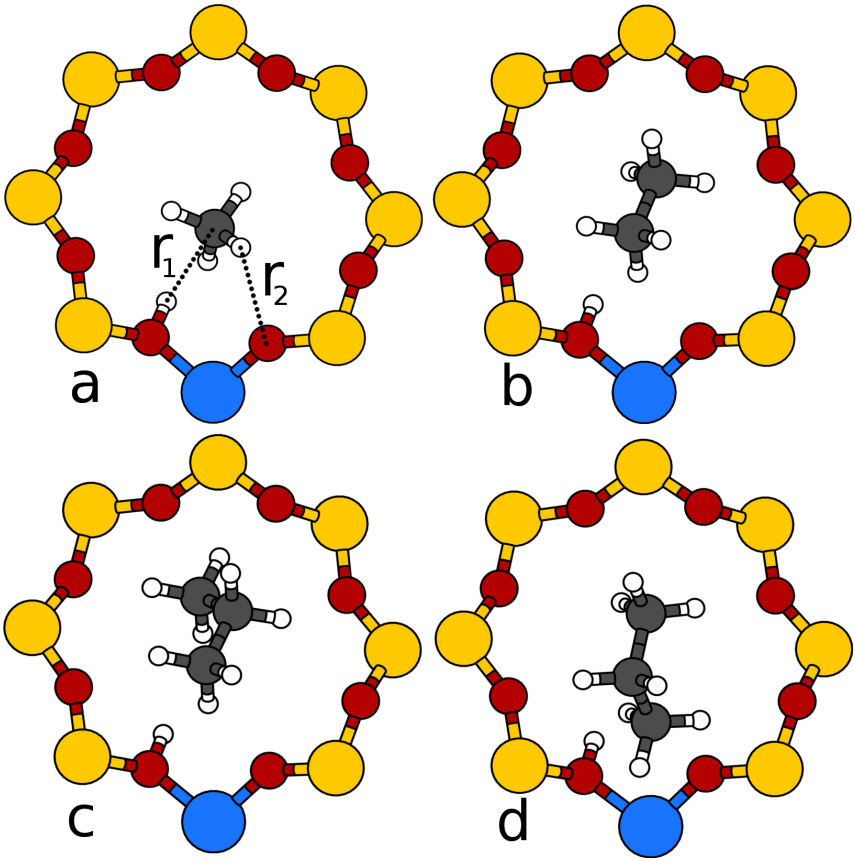

Figure 3.3: *Adsorption complexes of (**a**) methane, (**b**) ethane, (**c**) propane via primary carbon and (**d**) propane via secondary carbon with the acidic group at HO2 in an 8-membered ring of H-CHA.*

3.2 QM:QM Hybrid Optimization

3.2.1 Adsorption Structures in H-chabazite

The adsorption complexes of methane, ethane, and propane with the acidic active site of H-CHA have been pre-optimized using the conjugate-

Table 3.2: *Electronic energies, ΔE_e in kJ/mol, for adsorption of alkanes in H-CHA (θ =0.5). Re-optimization in normal mode coordinates vs. optimization in Cartesian coordinates.*

Alkane	PBE+D (this work)		PBE+D [6]	PW91 [30]
	Normal mode	Cartesian	Cartesian	Cartesian
methane	−34.77	−34.72	−32.32	−11
ethane	−47.02	−45.78	−43.42	−10
propane(C(1°))[a]	−58.89	−57.32	−59.44	−15
propane(C(2°))[b]	−58.04	−58.30	-	−11

[a] Propane adsorbed via primary carbon to hydroxyl group.
[b] Propane adsorbed via secondary carbon to hydroxyl group.

gradient algorithm implemented in VASP and subsequently refined using an optimization algorithm that uses normal-mode coordinates instead of Cartesians as described in the previous sections. Despite these optimized structures are very accurate, PBE+D is still not accurate enough to describe properly the correlation effects that are essential in describing adsorption. Therefore, each of the optimized structures discussed above have been refined using an hybrid approach combining high-level finite cluster MP2-CPC energies extrapolated at the infinite basis set limit using a localized atomic centered basis set with low-level cluster and periodic PBE+D energies using plane wave basis set within a subtractive QM:QM scheme [7, 131, 132, 150]. For the successive discussion, it is worth mentioning that the electronic and geometric structure of both the hybrid optimized systems (MP2/CPC-CBS(D,T):PBE+D) and the normal-mode optimized ones (PBE+D) used for the vibrational analysis do not correspond as they belong to two different PES. However, such a procedure is acceptable since the PBE+D PES curvature around the local minimum considered, determining the entity of the harmonic and anahrmonic frequencies, is enough accurate to get reliable results.

Table 3.3 reports the most relevant interatomic distances as in Table 3.1. Compared to the hybrid MP2:PBE+D results, PBE+D yields much shorter molecule surface distances in accord with substantial overbinding.

In addition to the total energies, Table 3.4 shows also the individual contributions to the hybrid QM:QM model for the adsorption structures

Table 3.3: *Relevant bond distances (pm) for adsorption complexes optimized at the PBE+D and hybrid MP2/CPC-CBS(D,T):PBE+D level.*

Alkane	PBE+D		MP2:PBE+D	
	r_1	r_2	r_1	r_2
methane	215	256	228	292
ethane	214	273	221	278
propane(C(1°))[a]	213	264	219	290
propane(C(2°))[b]	218	264	219	298

[a] Propane adsorbed via primary carbon to hydroxyl group.
[b] Propane adsorbed via secondary carbon to hydroxyl group.

Table 3.4: *Electronic adsorption energies obtained with the hybrid MP2/CPC-CBS(D,T): PBE+D method, and energy contributions for the periodic model, S, and the cluster model, C, obtained with different methods for alkane adsorption in H-CHA (kJ/mol). Long range and high level corrections, Δ_{LR}, and Δ_{HL}, respectively, are also given.*

		methane	ethane	propane	
				C(1°)[a]	C(2°)[b]
S(pbc)	PBE+D[c]	−34.72	−45.78	−57.32	−58.30
	PBE+D	−33.02	−44.15	−58.47	−56.89
	PBE	−8.08	−7.84	−7.84	−8.32
	D	−24.94	−36.31	−50.63	−48.57
Δ_{LR}	PBE+D	−3.98	−15.05	−24.78	−21.83
	PBE	0.53	−4.61	−5.66	−4.10
	D	−4.51	−10.44	−19.12	−17.73
C	MP2	−21.36	−21.17	−21.87	−22.30
Δ_{HL}		7.68	7.93	11.82	12.76
Total hybrid		−25.34	−36.21	−46.65	−44.13

[a] Propane adsorbed via primary carbon to hydroxyl group.
[b] Propane adsorbed via secondary carbon to hydroxyl group.
[c] At the PBE+D minimum.

considered. The MP2 energies for the cluster models lie all within 21.2 and 22.3 kJ/mol, and the chain length variation results from the long-range correction, Δ_{LR}, evaluated at the PBE+D level. The PBE+D results for the periodic model at the hybrid MP2:PBE+D structure hardly differ from the PBE+D energies for the structures optimized at this level. As it will be clear later, the hybrid level energies combined with the anharmonic corrections to the vibrational structure allow accurate estimations of the thermodynamic functions.

These two different optimizations play a very important role in the calculation of thermodynamics properties when chemical accuracy is the goal. On the one hand, the normal mode coordinates optimization allows a proper localization of the minimum ensuring in this way a stabilization of the vibrational structure. It is in fact common that standard optimization schemes are in many cases not able to give properly optimized structures, i.e. all the harmonic frequencies real. This feature is very common when looking for equilibrium structures of loosely bound complexes such as adsorbates or supramolecules. As already mentioned, plane wave periodic DFT suffers from numerical noise. Therefore, standard optimization techniques on a very flat PES can lead to several imaginary modes that affect strongly the accuracy in the calculation of the thermodynamic properties via partition function since such modes cannot be included in the sum. The implemented normal mode coordinates optimizer proved to be extremely accurate in many tests leading to an all-real set of harmonic frequencies.

On the other hand, since PBE+D is not accurate enough in describing non covalent interaction (such as molecular adsorption) with chemical, accuracy the corrections to the energies using explicitly correlated methods such as MP2 is fundamental. Optimizing the structure on the hybrid MP2:PBE+D PES allows an accurate localization of the minimum with a proper description of the dispersion interactions with reasonable computational times. As it will be clear later, this is step mandatory in calculating accurate quantum chemical enthalpies and free energies.

3.3 Normal Mode Frequency Calculation

In this section, the results of a frequency calculation via normal mode displacement are reported in detail, using both Cartesian and internal co-

ordinates distortions. The aim is to elucidate clearly the outcome of the numerical differentiation along the normal modes and how the increasing number of symmetric displacements determines the accuracy of the harmonic frequencies calculation. Moreover, the results validate at the same time the quality of the PES sampling along the normal mode coordinates. The example reported as test case is the so called *soft modes* region of the H-CHA model used in this work. This system is particularly suitable for testing these techniques since the *soft modes* regions of every zeolite system is characterized by many densely populated vibrational states. In addition, these modes are particularly low in energy. From the computational point of view, this means that the PES along such normal modes is particularly flat and, therefore, inaccuracies arising from the numerical noise are progressively more pronounced. Figure 3.4 illustrates how the use of more points in the numerical differentiation enhances the accuracy of the calculated frequencies. It shows the ratios of the frequencies calculated with 2-, 4- and 6-points with respect to the 8-point frequencies (considered as the best estimate) for the *soft modes* region of the unloaded H-CHA. The upper panel shows the results for the Cartesian coordinates distortions (eq. 2.16) while the lower one shows the results obtained by internal coordinates distortions (eq. 2.31). The frequency sets are converging while the number of points grows. The limit of 8-points displaced along each normal mode can be considered reasonably accurate.

It must be pointed out at this point that this is an accurate harmonic value for the given potential energy surface, obtained in this case by PW-DFT, PBE+D approach, which is not necessarily close to the experimental value. It rather means that the errors associated with the numerical noise become progressively negligible. Thus the estimation of the harmonic frequencies can be improved using more symmetric displacements without risking to explore meaningless regions of the PES, i.e. too far from the minimum or in the wrong direction. It confirms that the quality of the first Hessian matrix and its relative eigenvectors are a good guess and this particularly depends on the refinement due to the normal mode optimization. Last, the convergent behavior assesses the quality of the potential energy fit used to derive the anharmonic potential of eq. 2.18.

Figure 3.4 gives also information about the two different sampling procedure. It is clear that the distortions using internal coordinates are converging more regularly that the Cartesian ones. More symmetric points lead in the case of the internal coordinates distortions to a slightly higher

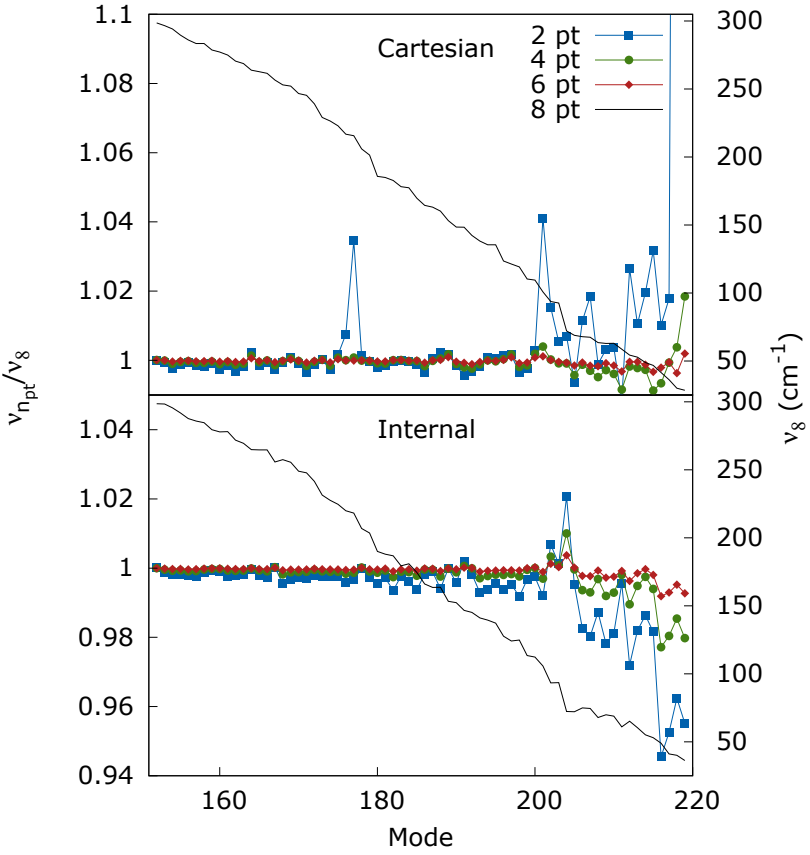

Figure 3.4: *Ratios between numerical frequencies calculated with 2-, 4-, and 6- points formulas and a reference set of frequencies (dashed line) calculated with an 8-point formula for the vibrations lower than 300 cm^{-1} in unloaded H-CHA. The upper panel refers to the results obtained using Cartesian coordinates distortions while the lower one refers to the results obtained using internal coordinates distortions.*

frequency as the ratio with between the 8-points result is generally smaller that 1. This trend is opposite in the case of Cartesian coordinates distor-

tion. The origin of this behavior is not fully clear but it can be associated with an inaccurate sampling along the normal mode. However, the deviations of the Cartesian distortions are extremely high if compared to the internal ones. As it will become clearer later, this significant lowering of the Cartesian coordinates distortion frequencies with an increasing number of points is not reflected in the resulting anharmonic frequencies. The latter are in most of the cases higher than the corresponding harmonic frequencies, meaning that the Cartesian sampling procedure faces limits when treating low frequency/high amplitude modes.

3.4 Anharmonic Frequency Calculation

Inclusion of anharmonic correction to the vibrational frequencies of a system is mandatory to reach chemical accuracy in the prediction of thermodynamic properties. This point is central to the discussion of this work and it will be shown that the consequences can be crucial. However, applying proper anharmonic corrections is not trivial and a certain attention must be paid to the outcome of the results which can be in some cases contradictory. As mentioned, the method adopted in this work to include anharmonicity is a variational scheme based on the solution of the Schrödinger equation for an Hamiltonian containing a sixth order model potential. To calculate this potential, the PES is sampled along the normal modes of vibration and fit to a sixth order polynomial. The choice of the coordinate system for making the proper sampling of the PES has been exposed theoretically in Section 2.8. Here follow two examples that show the consequences of this choice on the anharmonic frequencies. Later, the first applications to the thermodynamics of adsorption of two systems are presented.

3.4.1 Ethane Internal Rotation Mode

A typical case of failure of the harmonic approximation is the internal rotation of the two methyl groups in the ethane molecule which has been studied intensively with different approaches [152–156]. Here, a sinusoidal potential is approximated with a parabolic function which hardly describes the real situation. Using the variational approach to anharmonicity exposed in this work can solve the problem but the choice of

the proper displacement coordinate system determines the quality of the results.

Table 3.5 reports the harmonic and anharmonic frequencies for this internal rotation mode of ethane. The single point energies are calculated at the same level of theory (PW DFT, PBE+D, supercell).

Table 3.5: *Harmonic, ν, and anharmonic, ν^*, vibrational frequencies (cm^{-1}) for the internal rotation of ethane calculated using Cartesian and internal coordinates distortion.*

	Distortion	
	Cartesian	Internal
ν	313.6	298.2
ν^*	402.6	283.9

The frequencies at the harmonic level do not match, showing that the one calculated using internal coordinates distortions is lower than the Cartesian one. However, this discrepancy is not as significant as the difference in the results obtained applying the anharmonic corrections. The anharmonic frequency obtained by Cartesian distortions is by $89\,cm^{-1}$ higher than its corresponding harmonic value. This feature is in contradiction with the expected results, i.e. a lowering with respect to the harmonic vibrational frequency. In the case of the anharmonic frequency obtained by internal coordinates distortions, the frequency lowers by 14.3 cm^{-1}, getting very close to the experimental value ($289\,cm^{-1}$ [157]). To understand the origin of such a large discrepancy in these results visualizing the plot of the PES sampling along the normal mode of vibration gives already part of the answer. Figure 3.5 shows the plot of the potential energy single points along the internal rotation normal mode together with the corresponding sixth order fitted polynomial.

It is evident that the points of each of the two sampling approaches belong to two completely different PES as they never match. What is important to observe is that the set belonging to the internal coordinates distortions are always lower in energy with respect to the Cartesian set. At this point, the origin of the higher anharmonic frequency in the case of Cartesian coordinates distortion is clearer. However, this does not explain why the two sampling procedures give such different results. As discussed in detail in Section 2.8, the definition of normal mode coor-

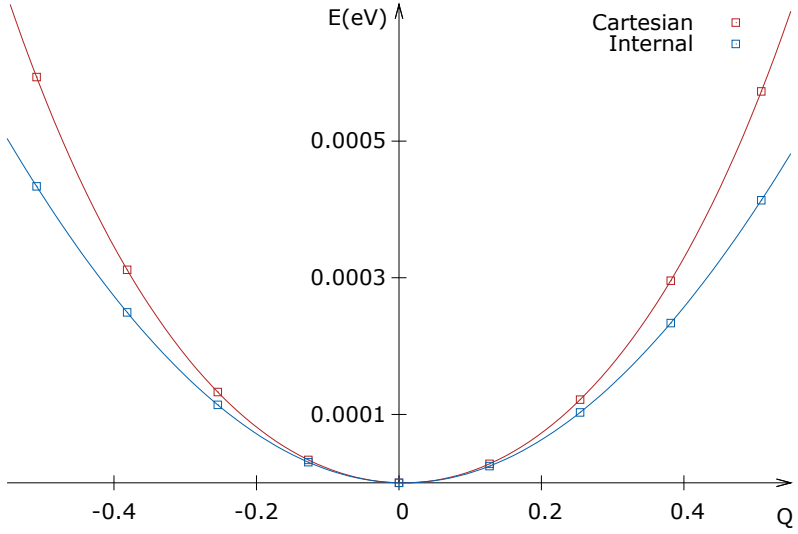

Figure 3.5: *Potential energy curve for the internal rotation mode of ethane sampled using Cartesian and internal coordinates distortions.*

dinates as linear combination of Cartesian coordinates is by construction valid for infinitesimal displacement only. Low frequency vibrations such as internal rotations have very large amplitude. This means that to explore the PES sufficiently, the steps used have to be relatively large. This leads to a strong coupling of the different vibrational coordinates [25, 26, 28, 29, 123], mixing up torsions with angle bends and stretching modes. To see the evidence of this fact, Figure 3.6 shows the plot of the averaged variation of the C—H bonds of the methyl groups from their equilibrium position during the sampling.

It is clear that the use of Cartesian displacement coordinates leads to a strong coupling between the torsional mode and all the C—H stretching modes of the methyl groups. Superposing Figure 3.6 and Figure 3.5, it is clear how this spurious variation of the C—H bond distance overlaps with the energy sampling determining a higher potential along the normal mode. The result of this coupling is the main origin of the results

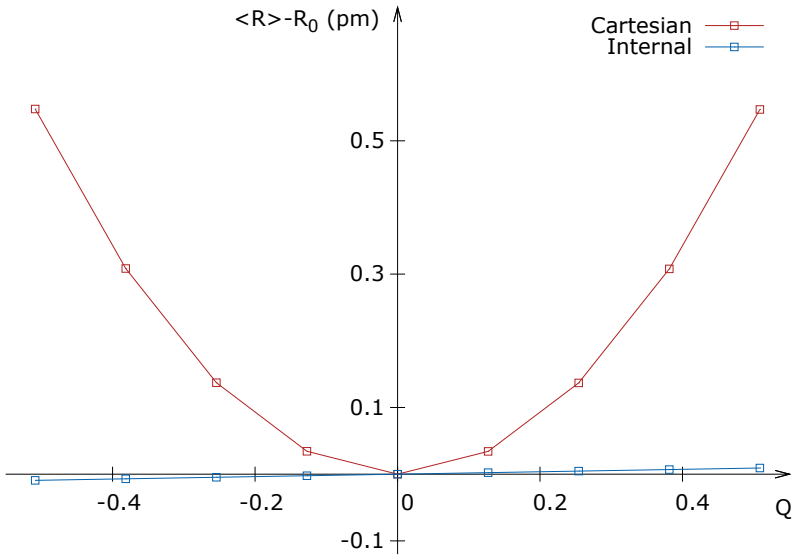

Figure 3.6: Average C—H bond length variation from the equilibrium position during the sampling along the internal rotation mode of ethane using Cartesian and internal coordinates distortions.

reported in Table 3.5. Small variations are observed also in the case of internal coordinates distortions. However, they are so insignificant that they do not affect the results of the anharmonic frequency calculation.

3.4.2 Methane Hindered Rotation Mode in H-chabazite

Having shown in the previous subsection the influence of the choice of the displacement coordinates system on a gas phase molecule low frequency mode, it will be now shown how this applies also in a more complex case. Molecular adsorption implies that the physisorbed molecule can still translate and rotate with respect to the surface or active site. However, these translations and rotations are no longer free as they take place within a potential generated by the crystal structure and they are treated in this work as vibrational modes. Such vibrations are commonly

called *hindered* translations and rotations since they retain a large contribution of original gas phase degrees of freedom. This motions imply that the molecule moves rigidly with respect to the surface or active site in a similar manner to the torsion of the methyl groups in the ethane molecule shown before. Such a motion is hardly reproduced by displacing the atoms along the normal mode using Cartesian coordinates distortions as they tend to couple many other vibrational modes. Therefore, the internal coordinates of the adsorbed molecule, especially if they involve light atoms like C−H bond, are not preserved and the sampling is an overlap of a hindered translation or rotation with bond stretching and angle bends.

To illustrate this, a hindered rotation mode has been selected for a methane molecule adsorbed in H-CHA (see model Section 1.3). This vibration consists in a rigid rotation of the methane molecule perpendicular to the O−H axis of the Brønsted acidic site. Figure 3.7 displays, as in the case of ethane, the averaged variation of the C−H bonds of the methane from their equilibrium position during the sampling.

Here, the influence of the coordinates system chosen to make the distortions along the normal mode is dramatic. The Cartesian displacements produce a very strong coupling with all the C−H bond distances which stretch by up to 0.5 pm. The effect on the aharmonic frequencies is consequently very large as reported in Table 3.6.

Table 3.6: *Harmonic, ν, and anharmonic, ν^*, vibrational frequencies (cm^{-1}) for a hindered rotation mode of methane in H-CHA calculated using Cartesian and internal coordinates distortion.*

	Distortion	
	Cartesian	Internal
ν	215.0	194.5
ν^*	286.1	185.9

Again, the shape of the plot of the two sampling along the normal mode reveals that two different PES directions have been explored as shown in Figure 3.8. It is also clear in this case that the PES sampled using Cartesian coordinates distortions does not represent the real picture for the specific normal mode.

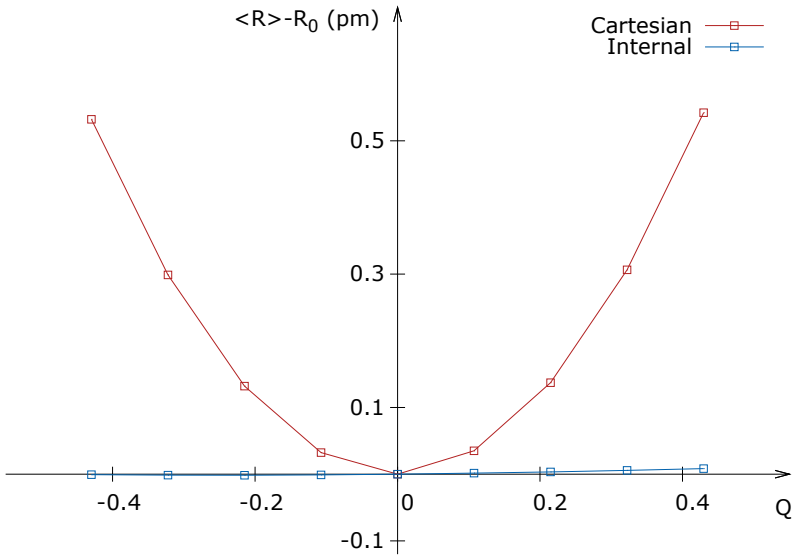

Figure 3.7: *Average C—H bond length variation from the equilibrium position during the sampling along a hindered rotation mode of methane in H-CHA using Cartesian and internal coordinates distortions.*

These errors in the estimate of the frequencies have a large impact on the accurate determination of the thermodynamic functions. Since entropy behaves asymptotically with frequencies approaching the zero, it is very sensitive to changes in the soft modes region. As it will be exposed in the next sections, apparently negligible inaccuracies in the frequency calculation lead to enormous deviation of the calculated thermodynamic functions with respect to the experimental values.

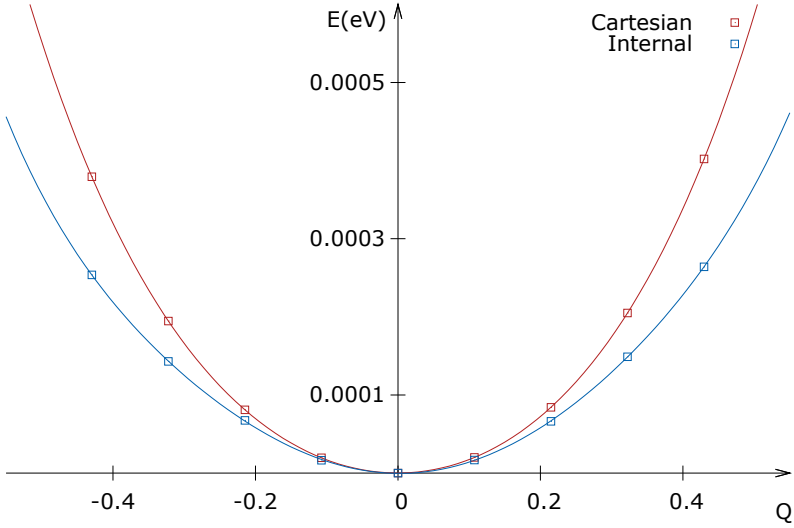

Figure 3.8: *Potential energy curve for a hindered rotation mode of methane in H-CHA sampled using Cartesian and internal coordinates distortions.*

3.5 Assessing the Accuracy of the Thermodynamic Functions

In this section, two cases of molecular adsorption are considered. The first one is the adsorption of methane in H-CHA at experimental conditions since zeolites are the main adsorbent materials of interest in this work. Moreover, this case has been intensively studied from the theoretical point of view partly due to the relatively small cell [6, 16, 30, 31, 131, 158–160]. The second case is the adsorption of methane on the MgO(001) surface at Ultra-High Vacuum (UHV) conditions. This case is particularly interesting since the methane molecules form a pure van der Waals monolayer on the MgO surface which has been studied both experimentally [38–43] and theoretically [44].

3.5.1 Methane Adsorption in H-chabazite

Due to the particular *soft* vibrational structure of zeolites [20–23], large amplitude motions not only occur for the molecule - active site vibrations but also for the crystal framework modes. Therefore, the description of normal modes in terms of internal coordinates is mandatory to sample the PES correctly. For each vibrational mode, a new set of accurate harmonic frequencies has been calculated using distortions of the normal mode in internal coordinates. 8 symmetric points are used and the Fornberg formulas [104] are applied. As previously [1], having this accurate sampling, the PES can be fit to a 6-th order polynomial and used to calculate anharmonic frequencies for all modes and thermodynamic functions.

To get an accurate estimate of the internal energy and enthalpy, the electronic energy differences are calculated at the minimum of the MP2/CPC-CBS(D,T):PBE+D potential energy surface (see Table 3.4).

Table 3.7 shows the thermodynamic functions for the adsorption of methane in acidic chabazite at experimental conditions (303 K, 0.1 MPa) for half coverage ($\theta = 0.5$). The method "Standard" refers to the results obtained using VASP conjugate-gradient optimization and Cartesian harmonic analysis. Comparison is made with the results obtained after refining the structure with the normal mode optimizer and calculating the vibrational partition function using harmonic frequencies resulting from Cartesian distortions (Cart) or from normal mode distortions (NM). In addition, results are compared with anharmonic frequencies obtained from rectilinear (anh-Cart) or from curvilinear distortions (anh-int). Thermal contributions to the total energies are derived from the translational, rotational and vibrational (harmonic and anharmonic) partition functions.

Figure 3.9 summarizes the results. The black solid line is the experimental value for methane adsorption on a sample of H-CHA (Al/Si = 1/14) and the grey bar around it represents the chemical accuracy "region" ($X_{Exp} \pm 1$ kcal/mol $\approx X_{Exp} \pm 4$ kJ/mol). The red full square is the MP2/CPC-CBS(D,T):PBE+D adsorption energy.

The results show that the anharmonic corrections affect the thermodynamic functions significantly. Entropy is extremely sensitive to such changes in the vibrational structure. There are large differences of almost 20 kJ/mol between the entropy term calculated using anharmonic frequencies with internal coordinate sampling (anh-int) and harmonic frequencies calculated in different ways (Standard, Cart, NM). This illus-

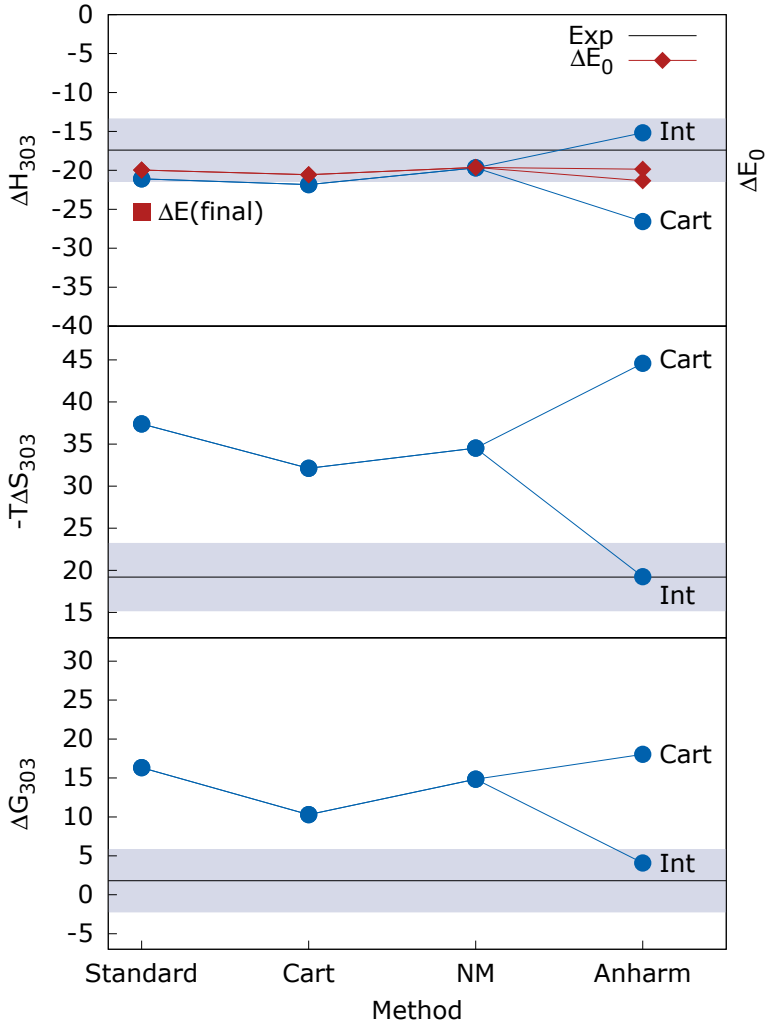

Figure 3.9: *Enthalpies, ΔH, entropy ,—TΔS and Gibbs free energies, ΔG, for adsorption of methane in H-CHA at experimental conditions (303 K, 0.1 MPa, θ =0.5) all in kJ/mol.*

Table 3.7: *Zero Point Corrected Energies, ΔE_0, Enthalpies, ΔH, Entropy Terms,$-T\Delta S$, and Gibbs Free Energies, ΔG, for Adsorption of Methane in H-CHA at Standard Conditions (303 K, 0.1 MPa, θ =0.5), all in kJ/mol.*

	Harmonic			Anharmonic		Exp.
	Standard[a]	Cart[b]	NM[b]	anh-Cart[b]	anh-int[b]	
ΔE_0	−19.95	−20.55	−19.62	−21.33	−19.85	-
ΔH	−21.08	−21.83	−19.68	−26.57	−15.17	−17.4
$-T\Delta S$[c]	37.40	32.13	34.53	44.60	19.25	19.2
ΔG	16.32	10.30	14.85	18.03	4.08	1.8

[a] Reference structure optimized using VASP conjugate-gradients.
[b] Reference structure optimized using normal mode coordinates.
[c] 43.56 and 12.94 kJ/mol due to loss of translational and rotational degrees of freedom respectively.

trates the failure of the harmonic oscillator model in describing weak and non-covalent bonding of the nuclei. This breakdown can be explained by the specifics of the adsorption process. When the adsorption complex is formed, the molecule looses its translational and rotational DOFs which are converted into vibrations. The translations and the rotations in the gas phase give to the system a higher entropy than the one resulting from the six molecule - surface vibrations. Therefore, adsorption is generally accompanied by a relatively high entropy loss. Describing the adsorption complex as a pure system of harmonic oscillators (especially for molecular- and physi-sorption) is definitely a rough approximation since the weak interactions of the molecule with the active site are far from being well represented by a mass-spring model. The results is a fictitiously large entropy loss becoming unreasonable when the temperature of the system increases i.e. when a strongly bound model for the adsorption complex becomes unrealistic.

Attention must be paid to the way the PES is sampled along the normal modes and the consequences that this can have on the thermodynamics [26]. The enthalpy and entropy differences between (anh-int) and (anh-Cart) are huge. The variational scheme proposed uses one-dimensional model potentials from a polynomial fit of the PES. As explained in the introduction, for large amplitude modes, rectilinear distortions are not

able to preserve the internal coordinates of the system unless infinitesimal steps are used. The result is a fictitious coupling of all the modes. Therefore, the PES is not sampled along the normal mode only, but receives contributions also from other coupled coordinates and this results in a potential well that is narrower than the starting harmonic one. This is the reason why anharmonic contributions from rectilinear PES sampling yield higher frequencies and, thus, lower vibrational entropies of the adsorption complex. This is avoided when the normal modes are expressed in curvilinear coordinates. The anharmonic corrections obtained this way go in the right direction and are very close to the experimental values. The deviations for the enthalpy, the entropy term $-T\Delta S$, and the Gibbs free energy are with 1.69, 0.05, and 2.28 kJ/mol all within chemical accuracy limits.

A final remark concerns the choice of the sets of internal coordinates employed. In this work, simple internals are used to describe covalent bonds such as bond stretches, angle bends and torsions, while for long-range interactions inverse power coordinates proposed by Baker and Pulay [122] are used. In most cases, even a redundant set of coordinates obtained from the topology of the system using standard covalent and van der Waals radii is not complete enough to describe specific vibrational modes. It is possible then to scale the covalent and van der Waals radii in order to include more internals able to describe a specific motion. Unfortunately, this procedure cannot be easily generalized and the user must pay attention to selecting a proper set of internals for some specific modes. As an empiric rule, it has been observed for this specific case that hindered rotational modes are better described when the covalent radius is expanded by 20-30%. This way, more bending and torsional coordinates are generated between the active site and the molecule able to describe the particular kind of motion. To model more accurately hindered translational modes, the van der Waals radius is expanded by 80-100% or more if needed. This partially ensures a proper motion of the adsorption complex keeping spurious contributions from other internal coordinates negligible. As mentioned, no general recipe can be applied to such problems and some chemical intuition is still needed to solve every specific cases. Even for small molecular cases, a proper set of internals has to be chosen accurately case by case [28, 29]. It is therefore clear that, for large systems the control of the user is more limited and many tests must be done in order to get an appropriate set. For some modes, the problems

are pathological and anharmonicity cannot be meaningfully treated. In these cases, simple harmonic frequencies are taken, but they are anyway a small minority in the whole set of frequencies.

3.5.2 Methane on the MgO(001) Surface

The theoretical study of the adsorption of a methane monolayer on the clean MgO(001) surface is challenging. On the one hand, magnesium oxide is an ionic crystal with a very stiff structure whose vibrational structure is relatively high in energy [161, 162]. The low frequency phonon region is not populated as in the case of zeolites and the methane monolayer modes are practically independent (uncoupled) from the crystal surface. Therefore, the use of rectilinear displacements is sufficient for sampling the PES of the normal mode vibrations of the bare MgO model surface. Nevertheless, particular attention must be paid to the choice of the set of redundant internal coordinates for the adsorption complex. The best choice proved to be a minimal set of valence type internal coordinates (i.e. 0% of covalent radii expansion) whereas the non-bonded type internal coordinates were determined expanding the van der Waals radii by 300% of their original values. This combination appeared to be the best compromise to describe both high frequency (intra-molecular and crystal) modes and low-frequency (inter-molecular monolayer and surface) modes.

For this system, the electronic energy difference at the minimum of the PES is taken from MP2:PBE+D + ΔCCSD(T) calculations of Tosoni and Sauer (Table 14 of ref. [44]). In Table 3.8, the PBE+D energy and the hybrid MP2:PBE+D + ΔCCSD(T) energy [44] are reported. The latter value is used for ΔE in this case whereas all nuclear motion contributions refer to the PBE+D potential energy surface.

Table 3.9 shows the thermodynamic functions related to the adsorption of a monolayer ($\theta = 1$) of methane on the MgO(001) surface at desorption conditions (47 K, 1.3×10^{-14} MPa). The nomenclature is the same as for Table 3.7. The column "Standard" is not present since no minimum (all real frequencies) was detected using standard optimization methods, conjugate-gradients method in this case. Therefore all the results reported refer to a minimum structure obtained by normal mode re-optimization [1]. Thermal contributions to the total energies are derived from the translational, rotational and vibrational (harmonic and anharmonic) partition functions.

Table 3.8: *Electronic Adsorption Energy for Adsorption of Methane on MgO(001) from MP2:PBE + ΔCCSD(T), PBE+D, PBE and Dispersion (D), all in kJ/mol (per Molecule).*

	Method[a]	ΔE_e
Tosoni & Sauer [44]	MP2:PBE+D + ΔCCSD(T)	−13.3
	PBE+D	−14.7
This work	PBE//PBE+D	−1.3
	D//PBE+D	−13.4

[a] "//" stands for "at the structure of".

Table 3.9: *Zero Point Corrected Energies, ΔE_0, Enthalpies, ΔH, Entropy Terms, $-T\Delta S$, and Gibbs Free Energies, ΔG, for Adsorption of Methane on MgO(001) Surface at Experimental Desorption Conditions (47 K, 1.3×10^{-14} MPa, θ =1), all in kJ/mol (per Molecule).*

	Harmonic		Anharmonic		Exp. [38]
	Cart[a]	NM[a]	anh-Cart[a]	anh-int[a]	
ΔE_0	−9.7	−9.8	−12.5	−13.4	-
ΔH	−10.7	−10.9	−13.7	−14.4	−12.2
$-T\Delta S$[b]	16.8	16.7	16.7	16.6	12.2 [c]
ΔG	6.1	5.8	3.0	2.1	0.0[c]

[a] Reference structure optimized using normal mode coordinates.
[b] 16.52 and 0.92 kJ/mol due to loss of translational and rotational degrees of freedom respectively.
[c] Assuming that at desorption temperature $\Delta G = 0$ and $T\Delta S = \Delta H$.

The results are summarized in Figure 3.10. As for the former case, the black solid line is the experimental value [38] and the grey bar around it represents the chemical accuracy "region". The red full square is the MP2:PBE+D + ΔCCSD(T) adsorption energy.

As for methane in H-CHA, the results obtained using anharmonic corrections with curvilinear displacements are in better agreement with the experimental results. It is very interesting that in this case, it is the zero point vibrational energy and enthalpy change that makes the difference between the results for different methods while the entropy term, due to the low temperature and pressure of the system, is not varying sensitively.

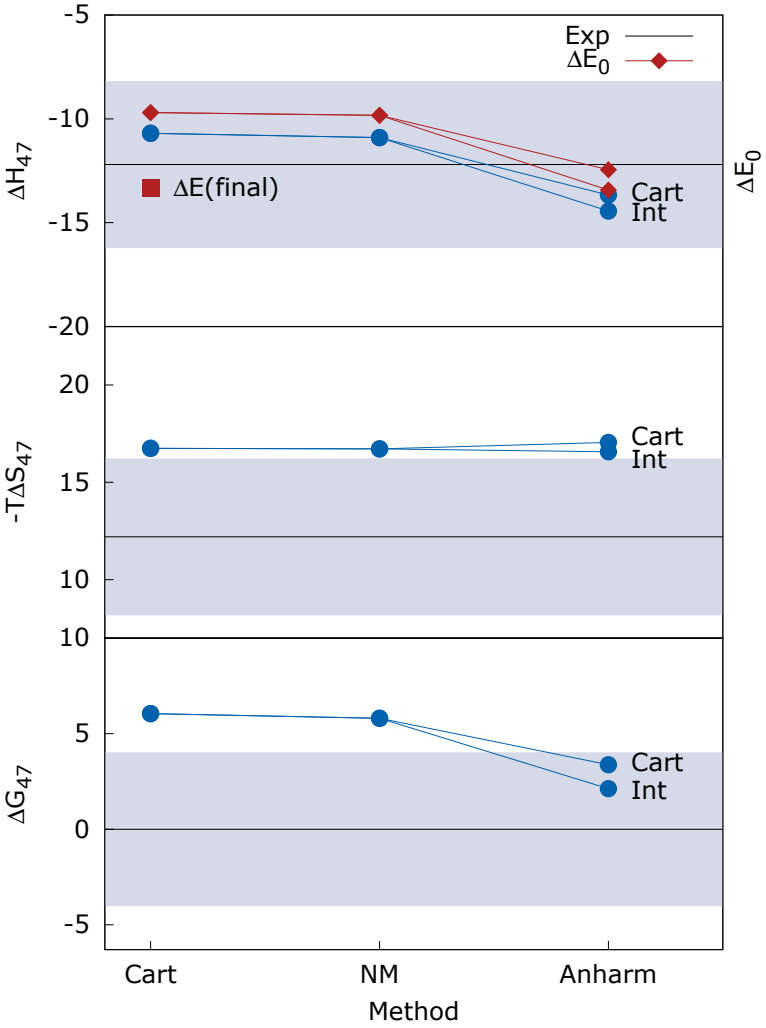

Figure 3.10: *Enthalpies, ΔH, entropy ,—TΔS and Gibbs free energies, ΔG, for adsorption of methane on MgO(001) surface at experimental desorption conditions (47 K, 1.3×10^{-14} MPa, θ = 1) all in kJ/mol (per molecule).*

The largest zero point vibrational energy changes are associated with the anharmonic results obtained with curvilinear displacements. In this case, the higher frequency modes make the largest contributions since they are drastically reduced by anharmonicity.

Since at low temperature and pressure the energy changes are not as large as for standard conditions, the capability of the method can be better appreciated analyzing the variation of ΔG with the temperature. The desorption temperature is defined as $\Delta G(T) = 0$. Figure 3.11 shows the Gibbs free energy calculated using different methods as a function of temperature. The black solid vertical line indicates the experimental desorption temperature (47 K) [38]. It separates the temperature range for which the desorption is favoured (gray region on its right) from the adsorption range. The result obtained with anharmonic corrections using curvilinear displacements (44 K) shows very good agreement with the experimental desorption temperature (47 K). The cartesian (Cart) and normal mode (NM) set of harmonic frequencies yield results that are very similar to the one obtained by Tosoni and Sauer [44] (see Table 3.10).

Table 3.10: *Desorption Temperatures (K),* T_{des}*, Activation Entropy Barriers (J/K mol),* $\Delta S^{\ddagger}$*, and Decimal Logarithm of the Prefactors* (s^{-1})*,* $\log\nu$*, for Adsorption of Methane on MgO(001) Calculated Using Different Methods.*

Method		T_{des}	$\Delta S^{\ddagger}$	$\log\nu$
Tosoni & Sauer[a]		33	−1.77	12.02
Harmonic	Cart	29	−1.86	12.52
	NM	30	−2.00	12.53
Anharmonic	Cart-disp	37	−2.10	12.59
	int-disp	44	−3.95	12.63
Exp. [38]		47	-	13.10

[a] Recalculated from the vibrational data of ref. [44].

Table 3.10 reports also the desorption activation entropy barriers and prefactors. Here, the entropy barrier is calculated taking the difference between the vibrational entropy of the adsorbed system and the vibrational entropy of the same system for which the rigid perpendicular vibrations of the eight adsorbed methane molecules have been removed from the partition function [44] (one vibration per adsorbed CH_4 molecule). The

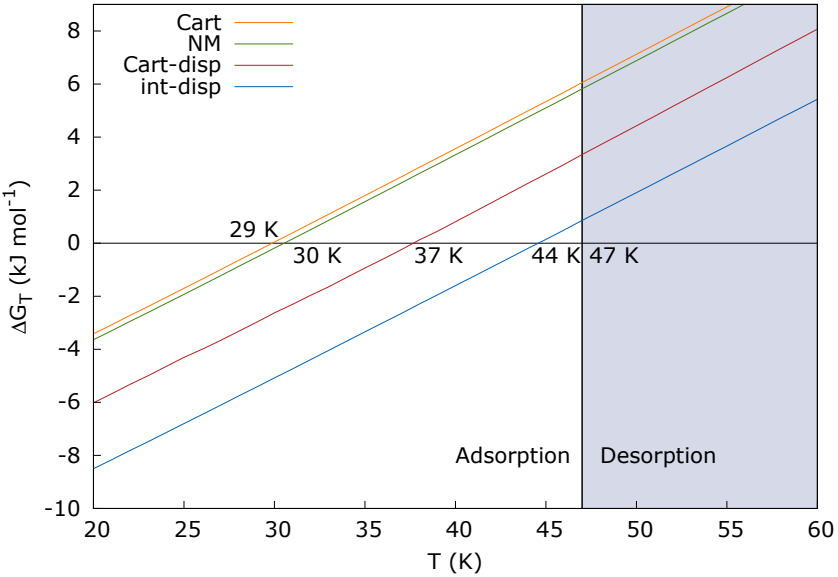

Figure 3.11: *Variation of Gibbs free energy (kJ/mol) calculated using different methods with respect to temperature.*

latter are considered as the reaction coordinates in transition state theory when applied to the desorption process. Having this activation barriers the prefactors are calculated as

$$\nu = \frac{k_B T}{\hbar} e^{\left(1 - \frac{\Delta S^{\ddagger}}{R}\right)} \tag{3.1}$$

where k_B is the Boltzmann constant, $\hbar$ the Planck constant and R the molar gas constant. As for the desorption temperature, the "anh-int" results show a better agreement with the experimental data reported in ref. [38].

3.6 Comparison with the Experiment

The aim of a new theoretical method or computational strategy is to reproduce with the highest possible accuracy the experimental results. If

this goal is achieved, theory and simulations can analyze the problem from the atomistic point of view and draw conclusions from "inside". The two cases exposed in the previous section are an example of how the method presented in this work is able to reproduce the results of two different experiments with chemical accuracy. Having matched the experimental results with the theoretical prediction allows to elucidate the nature of these processes from the molecular point of view since theory can look directly inside each single component. However, the ambition is to simulate a system and understand what is not understandable or not clear for the experimental results. For this purpose the results obtained applying the methods described and tested above to an adsorption experiment involving the series of the first three linear alkanes (methane, ethane and propane) in H-CHA are presented in this section. The challenge is to determine accurate enthalpies, entropies and Gibbs free energies of adsorption of each of the alkanes considered, but also to relate the thermodynamic consequences of the molecule - crystal interaction from the vibrational point of view. From the results of these calculations, it will be possible to understand what favors or not the adsorption of a molecule in a complex material such as an acidic zeolite. This will relate the *microscopic* geometric and vibrational structure of the adsorption complex to the *macroscopic* equilibrium thermodynamics.

3.6.1 Alkanes in H-chabazite

Having assessed the accuracy of the thermodynamics functions estimate applying the proposed computational protocol for methane adsorption in H-CHA, the study is extended to the series of the three first linear alkanes (methane, ethane, and propane) and directly compared with the experimental data. Table 3.11 shows the thermodynamic functions for the adsorption of the methane, ethane, and propane in H-CHA at experimental conditions (303 K for methane, 313 K for ethane and propane, 0.1 MPa) for half coverage ($\theta = 0.5$). Comparison is made with the results obtained from the calculation of the harmonic frequencies resulting from internal coordinates normal mode distortions (NM), to be considered as the best harmonic frequencies estimation, and anharmonic frequencies obtained from curvilinear distortions (anh-int). The results for methane adsorption are exactly the same as reported in Section 3.5.1. Thermal contributions to the total energies are derived from the translational, rotational and vi-

brational (harmonic or anharmonic) partition functions. As previously, while the frequencies are obtained from the PBE+D potential energy surface, the electronic energies are the hybrid MP2/CPC-CBS(D,T):PBE+D calculations (see Table 3.4). The calculated thermodynamic functions are compared with measured values for methane, ethane, and propane. The effect of anharmonicity on the entropy term is enormous, of the order of 15 to 20 kJ/mol. A very large effect is also seen for the thermal enthalpy contributions, which increase from about 0.5 kJ/mol to 4.7 (methane), 3.2 (ethane), and 4.6 (propane) kJ/mol. The thermodynamic functions calculated using anharmonic frequencies with internal coordinate distortions for methane, ethane and propane adsorbed with the primary carbon are all reproducing the experimental data within chemical accuracy, i.e. within ± 1 kcal/mol $\approx \pm 4.2$ kJ/mol, as Figure 3.12 illustrates. The plots show the experimental data points (red diamonds) with the experimental error bars of $\pm$ 4.184 kJ/mol and the calculated ones.

The results for propane adsorption via secondary carbon have been excluded from Figure 3.12 because they deviate significantly from the experimental data with respect to the entropy term and consequently to the Gibbs free energy. Such a discrepancy cannot be associated with some inaccuracy of the method but must be due to the structure and conformation of the adsorption complex itself. Due to the strong interaction of the propane methyl groups with the zeolite framework, highly entropic motions such as hindered translations and rotations are way stiffer than in the case of primary carbon adsorption, resulting in a drastic lowering of the entropic term for the adsorption complex. The result is a destabilization of the adsorbed state favoring adsorption via the primary carbon atom. This feature has been also observed in molecular dynamics simulations. Bučko et al. [30] have shown that the probability of adsorbing a propane molecule in H-CHA via a primary carbon atom is about 19 times higher than adsorbing it via a secondary one. The Boltzmann population analysis calculated from the absolute Gibbs free energies for propane adsorption via primary and secondary carbon shows that the population of the propane adsorbed with primary carbon is 200 larger than the secondary carbon one. From the present results reported, it is clear that the origin of this unfavorable adsorption configuration is entropic as the enthalpy does not vary strongly depending on the structure of the adsorption complex. Here, the effect of the anharmonicity on the adsorption entropy is evident. The low frequency/large amplitude modes associated

Table 3.11: *Zero point corrected energies, ΔE_0, enthalpy, ΔH, entropic term, $-T\Delta S$, and Gibbs free energy, ΔG, for the adsorption of methane, ethane, and propane in H-CHA at experimental conditions (303 K for methane, 313 K for ethane and propane, 0.1 MPa, θ=0.5) calculated using harmonic internal coordinates normal mode distortions (NM), anharmonic internal coordinates distortions (anh-int), and experimental data (all in kJ/mol).*

	methane			ethane		
	NM	anh-int	Exp.	NM	anh-int	Exp.
ΔE_0	−19.62	−19.85	-	−33.78	−33.41	-
ΔH	−19.68	−15.17	−17.4	−33.10	−30.18	−27.5
$-T\Delta S$	34.53	19.25	19.2	37.42	23.28	23.8
ΔG	14.86	4.09	1.8	4.31	−6.90	−3.7
	propane					
	C(1°)			C(2°)		
	NM	anh-int	Exp.	NM	anh-int	Exp.
ΔE_0	−42.56	−45.06	-	−42.62	−42.2	-
ΔH	−42.70	−40.47	−37.6	−39.73	−38.96	−37.6
$-T\Delta S$	48.31	28.22	27.5	42.55	40.49	27.5
ΔG	5.61	−12.26	−10.1	2.82	1.52	−10.1

with the hindered translations and rotations of the adsorbed molecule, the floppy vibrations of the zeolites framework, and also the possible internal rotations of methyl groups in ethane and propane are far from being properly described by a parabolic model potential.

The accurate estimate of the adsorbed state entropy given by treating all the vibrations as anharmonic is key to understanding why zeolites are such excellent adsorbent materials. The floppy vibrational structure of zeolites [20–23] is known to be central in favoring the diffusion of molecules into the pores [158, 163]. In this work, it is shown that this feature is favoring also adsorption in a direct way. Since soft vibrations can couple with the surface modes of the adsorption complex, due to the strong long range interactions, the vibrational structure of the whole crystal framework changes consistently with the presence of the adsorbate. This means that the crystal adapts its structure to accommodate the molecule weak-

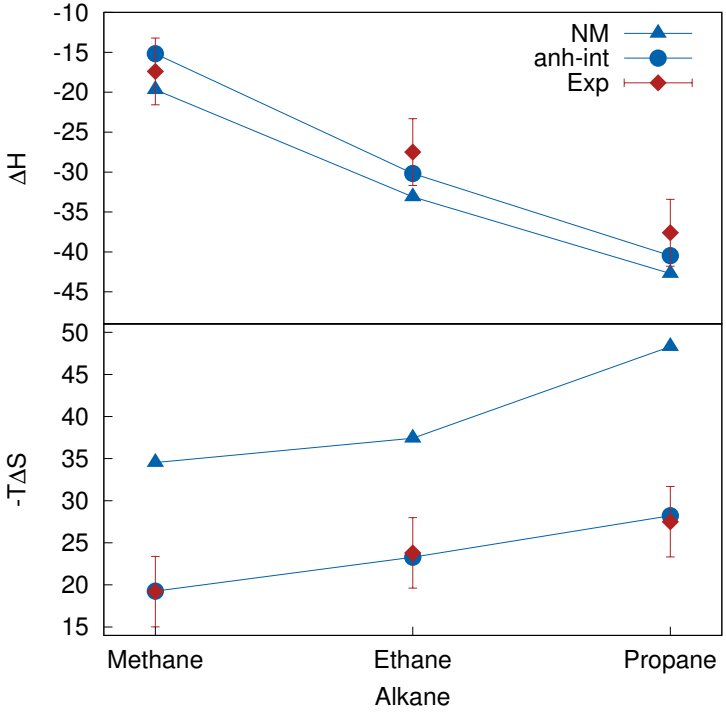

Figure 3.12: *Enthalpy, ΔH, entropic term, −TΔS, and Gibbs free energy, ΔG, for the adsorption of methane, ethane and propane in H-CHA at experimental conditions (303 K for methane, 313 K for ethane and propane, 0.1MPa, θ=0.5) calculated using harmonic internal normal mode distortions (NM), anharmonic internal coordinates distortions (anh-int), and experimental data (all in kJ/mol).*

ening the strength of some bonded interactions (mainly collective angle bending and torsions) and giving rise to a highly entropic adsorbed state. The correlation of adsorption entropy and enthalpy with respect to the zeolite framework topology has been studied intensively in the past [164]. The experimental observations show that the tighter the pore structure the higher the adsorption enthalpy and entropy for the same alkane con-

sidered in various zeolites (e.g. H-MFI > H-MOR > H-FAU). However, whereas the enthalpy trend can be reasonably explained with bare dispersion interactions arguments (more lateral interactions with the framework), the nature of the entropy change was not completely understood. In this work, this feature is made clear from the vibrational point of view since the zeolites vibrational structure is affected strongly by the presence of the adsorbed molecule mediated by dispersion interactions. Therefore, a zeolite topology that favors adsorption should have enough tight pores to produce strong dispersion interactions (i.e. high enthalpy gain) but also rather low strained structural motifs, such as high membered rings, to ensure a specific vibrational "floppiness" that allows the structure to adapt during adsorption (i.e. low entropy loss). Some information on the type of vibrations involved in such low frequency modes are drawn from comparison with simple adsorption models proposed by Tait et al. [38]. For the desorption of linear alkanes from the MgO(100) surface, the Gibbs free energies have been calculated (i) for an immobile adsorbate model, where no translations or rotations are allowed in the adsorbed state, (ii) for a rotating adsorbate, where only rotations along the adsorbate principal axis of inertia are allowed (3 for a non-linear molecule), and (iii) for a mobile adsorbate, where 2D translations and a specific number of rotations are allowed depending on the nature of the molecule [38]. In this case, this number is 3 for methane, 2 for ethane, and 1 for propane.

Figure 3.13 shows the results for the Gibbs free energy including the latter calculated using the simple adsorption models described above. It is clear from the picture that the experimental and anharmonic results are in very good agreement with the mobile model. In other words, the most disordered (entropic) model describes better the nature of the physisorption. Moreover, it confirms that the anharmonic treatment of the vibrations is able to give a more realistic picture of the molecule - active site relative motion being close to the mobile model as well.

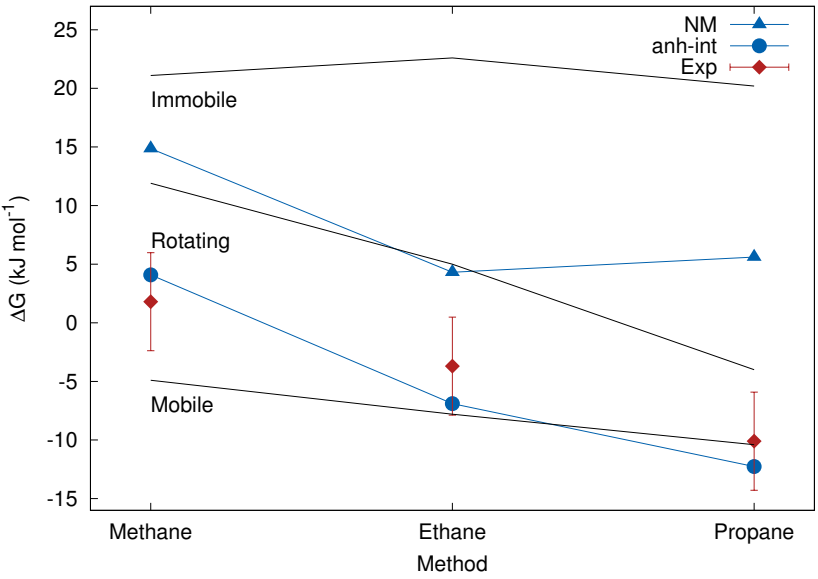

Figure 3.13: *Gibbs free energy, ΔG, for the adsorption of methane, ethane and propane in H-CHA at experimental conditions (303 K for methane, 313 K for ethane, and propane, 0.1MPa, θ=0.5) calculated using harmonic internal normal mode distortions (NM), anharmonic internal coordinates distortions (anh-int), experimental data, and simplified adsorption models (black dashed lines for Immobile, Rotating and Mobile models respectively).*

4 Conclusions

Due to numerical accuracy limits, plane wave DFT calculations may have difficulties to tightly converge energy minimum structures for systems with flat potential energy surfaces as indicated by oscillations of energy and structure parameters. Another indication of numerical instabilities is the presence of small imaginary frequencies when trying to characterize the stationary points as minima or saddle points. These difficulties can be overcome by a refinement optimization step in which normal mode coordinates instead of Cartesian coordinates are used. Displacements in normal mode coordinates are also recommended when calculating harmonic vibrational frequencies from finite differences of energy gradients. The harmonic frequencies using central displacements along normal modes show a convergent behavior when enlarging the number of symmetrically placed points. When harmonic frequencies obtained this way are used to calculate vibrational contributions instead of frequencies obtained with Cartesian distortions after optimization in Cartesian coordinates, the free energies of adsorption of small alkanes as a function of the carbon number show a much more regular behavior in agreement with the trend of the experimental results. The ab initio enthalpies, entropies and free energies of adsorption calculated from vibrational partition functions using anharmonic corrections show agreement with the experimental data within the chemical accuracy limit ($\pm$4.2 kJ/mol) if curvilinear displacements along normal modes are used. The proper sampling of the PES to get the one-dimensional anharmonic model potential proved to be essential for an accurate determination of thermodynamic functions. Simple harmonic frequencies, even when estimated with high accuracy (e.g. displacing the structure along normal modes if numerical derivatives are unavoidable), are not good enough to describe non-bonded interactions. As expected, anharmonic corrections enhance the vibrational entropy of the adsorption complex and, thus, favor adsorption.

For systems with very low desorption temperatures as methane on

MgO(001), anharmonicity is found to cause significant changes on zero point vibrational energies and, thus, on the enthalpy as it lowers the higher vibrational wavenumbers. Anharmonicity effects change the adsorption energy at 0 K from 9.8 to 13.4 kJ/mol, and the heat of adsorption at 47 K from 10.9 to 14.4 kJ/mol. After inclusion of anharmonicity effects the ab initio Gibbs free energy deviates by +2.1 kJ/mol from the experimental data, showing that ab initio calculations yield Gibbs free energies within chemical accuracy limits.

The adsorption of methane, ethane, and propane in H-CHA proved how important is the location of a well relaxed structure, using normal mode coordinates re-optimization, and the inclusion of anharmonicity to recast the trend of the experimental observations. It is clear that harmonic frequencies, although estimated at a very accurate level using up to 8-point symmetric numerical differences along the normal modes, are describing properly the high entropy state of the adsorption complex. Moreover, the results show that not even the experimental trend is reproduced by the calculation of the thermodynamic functions using this set of frequencies. The inclusion of anharmonicity effects reproduces with high fidelity the experimental results both in the trend and in the exact values within chemical accuracy limits. The ab initio Gibbs free energies deviate by 3.0, -3.2 and -2.2 kJ/mol from the experimental data for methane, ethane and propane adsorbed with primary carbon. From the calculated enthalpies, entropies, and Gibbs free energies it is clear that adsorption of propane via secondary carbon is not favored and the reason of this behavior is purely entropic. In fact, the adsorption enthalpy for this adsorption configuration in very similar to the case of propane adsorbed via primary carbon while the entropic term deviates by 13.0 kJ/mol from the experimental value. It is then possible to conclude that the adsorption of propane via secondary carbon is unfavored because the higher interaction of the two methyl groups with the walls of the zeolite cage makes the molecule - active site vibrations stiffer i.e. increases absolute entropy of the adsorbed system.

Concluding Remarks

The computational strategy presented in this work aims at solving the problems involved in the atomistic study of adsorption thermodynam-

ics. The presented fully quantum mechanical ab initio approach combined with statistical mechanics for deriving the thermodynamic functions must not be seen to be in opposition to ab initio molecular dynamics but rather as a complementary. The presented method allows to study the problem from a different point of view and draws conclusions that cannot be reached using molecular dynamics. Many results coming from the two different approaches agree qualitatively and in some cases also quantitatively. On the one hand, if molecular dynamics ideally allows to explore all the possible thermodynamic states of a system at a given temperature, the final results coming from the simulation are at the end an average of many pieces of information. Therefore, a detailed analysis of some specific phenomena can be rather difficult if not impossible. On the other hand, calculating the vibrational partition functions for a system located at only one of the possible minimum energy structures at finite temperature can give a a completely wrong picture of the thermodynamics, especially if the harmonic approximation is used without taking into account its limitations. However, this work shows that sampling the PES along a set of normal mode coordinates allows to explore it in a more detailed way in order to include a more realistic representation of the vibrational structure into the vibrational partition function. This approach allowed to explain the origin of adsorption from the vibrational point of view. It opens the possibility to understand the underlying nature of an apparently contradictory result, the unfavorable adsorption of propane via secondary carbon, by direct analysis of the vibrational structures. As mentioned, this result has been observed also in molecular dynamics simulation, however, in that case, the origin of such a behavior could not be explained quantitatively as it has been done in the present work.

Although at present computational chemistry and material science are far from being able to afford a rational design of new molecules, materials or drugs, it can be definitely stated that the theoretical and computational predictions reached a sufficient level of accuracy to point the direction in which experiments should go. The challenge is to bring the theory and the efficiency of the computation at a level that allows to combine the results consistently with the experimental work in order to reduce as much as it can be the time-consuming step of trial and error in the research and optimization of novel materials. This is the hope, the rest is work to be done.

Bibliography

[1] G. Piccini and J. Sauer, "Quantum chemical free energies: Structure optimization and vibrational frequencies in normal modes," *J. Chem. Theory Comput.*, vol. 9, no. 11, pp. 5038–5045, 2013.

[2] G. Piccini and J. Sauer, "Effect of anharmonicity on adsorption thermodynamics," *J. Chem. Theory Comput.*, vol. 10, no. 6, pp. 2479–2487, 2014.

[3] G. Piccini, M. Alessio, J. Sauer, Y. Zhi, Y. Liu, R. Kolvenbach, A. Jentys, and J. A. Lercher, "Accurate adsorption thermodynamics of small alkanes in zeolites. ab initio theory and experiment for h-chabazite," *J. Phys. Chem. C*, vol. 119, pp. 6128–6137, 03 2015.

[4] C. J. Cramer, *Essentials of Computational Chemistry: Theories and Models*. Wiley, 2004.

[5] F. Claeyssens, J. N. Harvey, F. R. Manby, R. A. Mata, A. J. Mulholland, K. E. Ranaghan, M. Schütz, S. Thiel, W. Thiel, and H.-J. Werner, "High-accuracy computation of reaction barriers in enzymes," *Angew. Chem. Int. Ed.*, vol. 45, no. 41, pp. 6856–6859, 2006.

[6] F. Goltl, A. Gruneis, T. Bučko, and J. Hafner, "Van der waals interactions between hydrocarbon molecules and zeolites: Periodic calculations at different levels of theory, from density functional theory to the random phase approximation and møller-plesset perturbation theory," *J. Chem. Phys.*, vol. 137, no. 11, p. 114111, 2012.

[7] N. Hansen, T. Kerber, J. Sauer, A. T. Bell, and F. J. Keil, "Quantum chemical modeling of benzene ethylation over H-ZSM-5 approaching chemical accuracy: A hybrid MP2:DFT study," *J. Am. Chem. Soc.*, vol. 132, no. 33, pp. 11525–11538, 2010.

[8] S. Svelle, C. Tuma, X. Rozanska, T. Kerber, and J. Sauer, "Quantum chemical modeling of zeolite-catalyzed methylation reactions: Toward chemical accuracy for barriers," *J. Am. Chem. Soc.*, vol. 131, no. 2, pp. 816–825, 2009.

[9] K. Sillar, A. Hofmann, and J. Sauer, "Ab initio study of hydrogen adsorption in MOF-5," *J. Am. Chem. Soc.*, vol. 131, no. 11, pp. 4143–4150, 2009. PMID: 19253977.

[10] K. Sillar and J. Sauer, "Ab initio prediction of adsorption isotherms for small molecules in metal–organic frameworks: The effect of lateral interactions for methane/CPO-27-Mg," *J. Am. Chem. Soc.*, vol. 134, no. 44, pp. 18354–18365, 2012.

[11] A.-P. E. Kunz, H. Liu, and W. F. van Gunsteren, "Enhanced sampling of particular degrees of freedom in molecular systems based on adiabatic decoupling and temperature or force scaling," *J. Chem. Phys.*, vol. 135, no. 10, 2011.

[12] T. H. Rod and U. Ryde, "Accurate QM/MM free energy calculations of enzyme reactions: methylation by catechol o-methyltransferase," *J. Chem. Theory Comput.*, vol. 1, no. 6, pp. 1240–1251, 2005.

[13] T. H. Rod and U. Ryde, "Quantum mechanical free energy barrier for an enzymatic reaction," *Phys. Rev. Lett.*, vol. 94, p. 138302, Apr 2005.

[14] B. A. De Moor, M.-F. Reyniers, and G. B. Marin, "Physisorption and chemisorption of alkanes and alkenes in H-FAU: A combined ab initio-statistical thermodynamics study," *Phys. Chem. Chem. Phys.*, vol. 11, pp. 2939–2958, 2009.

[15] B. A. De Moor, M.-F. Reyniers, O. C. Gobin, J. A. Lercher, and G. B. Marin, "Adsorption of C2C8 n-alkanes in zeolites," *J. Phys. Chem. C*, vol. 115, no. 4, pp. 1204–1219, 2011.

[16] B. A. De Moor, A. Ghysels, M.-F. Reyniers, V. Van Speybroeck, M. Waroquier, and G. B. Marin, "Normal mode analysis in zeolites: Toward an efficient calculation of adsorption entropies," *J. Chem. Theory Comput.*, vol. 7, no. 4, pp. 1090–1101, 2011.

[17] P. Hobza, J. Sauer, C. Morgeneyer, J. Hurych, and R. Zahradnik, "Bonding ability of surface sites on silica and their effect on hydrogen bonds. a quantum-chemical and statistical thermodynamic treatment," *J. Phys. Chem.*, vol. 85, no. 26, pp. 4061–4067, 1981.

[18] G. Kresse and J. Hafner, "Ab initio molecular dynamics for liquid metals," *Phys. Rev. B*, vol. 47, no. 1, pp. 558–561, 1993.

[19] M. Johnson, K. Parlinski, I. Natkaniec, and B. Hudson, "Ab initio calculations and INS measurements of phonons and molecular vibrations in a model peptide compound – urea," *Chem. Phys.*, vol. 291, no. 1, pp. 53–60, 2003.

[20] M. T. Dove, M. J. Harris, A. C. Hannon, J. M. Parker, I. P. Swainson, and M. Gambhir, "Floppy modes in crystalline and amorphous silicates," *Phys. Rev. Lett.*, vol. 78, no. 6, pp. 1070–1073, 1997.

[21] K. D. Hammonds, H. Deng, V. Heine, and M. T. Dove, "How floppy modes give rise to adsorption sites in zeolites," *Phys. Rev. Lett.*, vol. 78, no. 19, pp. 3701–3704, 1997.

[22] K. D. Hammonds, V. Heine, and M. T. Dove, "Rigid-unit modes and the quantitative determination of the flexibility possessed by zeolite frameworks," *J. Phys. Chem. B*, vol. 102, no. 10, pp. 1759–1767, 1998.

[23] M. T. Dove, V. Heine, and K. D. Hammonds, "Rigid unit modes in framework silicates," *Mineralog. Mag.*, vol. 59, no. 397, pp. 629–639, 1995.

[24] A. Beste, "One-dimensional anharmonic oscillator: Quantum versus classical vibrational partition functions," *Chem. Phys. Lett.*, vol. 493, no. 1–3, pp. 200 – 205, 2010.

[25] J. A. Boatz and M. S. Gordon, "Decomposition of normal-coordinate vibrational frequencies," *J. Phys. Chem.*, vol. 93, no. 5, pp. 1819–1826, 1989.

[26] B. Njegic and M. S. Gordon, "Exploring the effect of anharmonicity of molecular vibrations on thermodynamic properties," *J. Chem. Phys.*, vol. 125, no. 22, p. 224102, 2006.

[27] B. Njegic and M. S. Gordon, "Predicting accurate vibrational frequencies for highly anharmonic systems," *J. Chem. Phys.*, vol. 129, no. 16, p. 164107, 2008.

[28] N. De Silva, B. Njegic, and M. S. Gordon, "Anharmonicity of weakly bound M+-H_2 complexes," *J. Phys. Chem. A*, vol. 115, no. 15, pp. 3272–3278, 2011.

[29] N. De Silva, B. Njegic, and M. S. Gordon, "Anharmonicity of weakly bound Li+–$(H_2)_n$ (n = 1–3) complexes," *J. Phys. Chem. A*, vol. 116, no. 49, pp. 12148–12152, 2012.

[30] T. Bučko, L. Benco, J. Hafner, and J. G. Ángyán, "Proton exchange of small hydrocarbons over acidic chabazite: Ab initio study of entropic effects," *J. Catal.*, vol. 250, no. 1, pp. 171 – 183, 2007.

[31] M. Sierka and J. Sauer, "Proton mobility in chabazite, faujasite, and ZSM-5 zeolite catalysts. comparison based on ab initio calculations," *J. Phys. Chem. B*, vol. 105, no. 8, pp. 1603–1613, 2001.

[32] C. S. Lo, R. Radhakrishnan, and B. L. Trout, "Application of transition path sampling methods in catalysis: A new mechanism for CC bond formation in the methanol coupling reaction in chabazite," *Catal. Today*, vol. 105, no. 1, pp. 93 – 105, 2005.

[33] X. Solans-Monfort, M. Sodupe, V. Branchadell, J. Sauer, R. Orlando, and P. Ugliengo, "Adsorption of NH_3 and H_2O in acidic chabazite. comparison of ONIOM approach with periodic calculations," *J. Phys. Chem. B*, vol. 109, no. 8, pp. 3539–3545, 2005. PMID: 16851391.

[34] I. M. Dahl, H. Mostad, D. Akporiaye, and R. Wendelbo, "Structural and chemical influences on the MTO reaction: A comparison of chabazite and SAPO-34 as MTO catalysts," *Micropor. Mesopor. Mater.*, vol. 29, no. 1–2, pp. 185 – 190, 1999.

[35] B. M. Lok, C. A. Messina, R. L. Patton, R. T. Gajek, T. R. Cannan, and E. M. Flanigen, "Silicoaluminophosphate molecular sieves: Another new class of microporous crystalline inorganic solids," *J. Am. Chem. Soc.*, vol. 106, no. 20, pp. 6092–6093, 1984.

[36] B. Vora, J. Q. Chen, A. Bozzano, B. Glover, and P. Barger, "Various routes to methane utilization - SAPO-34 catalysis offers the best option," *Catal. Today*, vol. 141, pp. 77–83, 3 2009.

[37] C. T. Campbell and J. R. V. Sellers, "The entropies of adsorbed molecules," *J. Am. Chem. Soc.*, vol. 134, no. 43, pp. 18109–18115, 2012.

[38] S. L. Tait, Z. Dohnalek, C. T. Campbell, and B. D. Kay, "n-alkanes on MgO(100). ii. chain length dependence of kinetic desorption parameters for small n-alkanes," *J. Chem. Phys.*, vol. 122, no. 16, p. 164708, 2005.

[39] D. R. Jung, J. Cui, and D. R. Frankl, "Dynamics and kinetics of monolayer CH_4 on MgO(001) studied by helium-atom scattering," *Phys. Rev. B*, vol. 43, pp. 10042–10050, May 1991.

[40] J. Larese, "Neutron scattering studies of the structure and dynamics of methane absorbed on MgO(100) surfaces," *Phys. B: Condensed Matter*, vol. 248, no. 1–4, pp. 297 – 303, 1998.

[41] A. Freitag and J. Z. Larese, "Layer growth of methane on MgO:an adsorption isotherm study," *Phys. Rev. B*, vol. 62, pp. 8360–8365, Sep 2000.

[42] J. Z. Larese, D. M. y Marero, D. S. Sivia, and C. J. Carlile, "Tracking the evolution of interatomic potentials with high resolution inelastic neutron spectroscopy," *Phys. Rev. Lett.*, vol. 87, p. 206102, Oct 2001.

[43] T. Arnold, R. E. Cook, S. Chanaa, S. M. Clarke, M. Farinelli, P. Yaron, and J. Larese, "Neutron scattering and thermodynamic investigations of thin films of n-alkanes adsorbed on MgO(100) surfaces," *Phys. B: Condensed Matter*, vol. 385–386, Part 1, no. 0, pp. 205 – 207, 2006. Proceedings of the Eighth International Conference on Neutron Scattering.

[44] S. Tosoni and J. Sauer, "Accurate quantum chemical energies for the interaction of hydrocarbons with oxide surfaces: CH4/MgO(001)," *Phys. Chem. Chem. Phys.*, vol. 12, no. 42, pp. 14330–14340, 2010.

[45] H. Lüth, *Solid Surfaces, Interfaces and Thin Films*. Springer-Verlag, 2010.

[46] K. Oura, V. Lifshits, A. Saranin, and A. Zotov, *Surface Science: An Introduction*. Advanced Texts in Physics, Springer Berlin Heidelberg, 2010.

[47] D. of Chemical Nomenclature, S. R. I. U. of Pure, A. Chemistry, M. Nic, J. Jirat, and B. Kosata, *Iupac Goldbook*. IUPAC, 2006.

[48] J. Sauer, P. Ugliengo, E. Garrone, and V. R. Saunders, "Theoretical study of van der waals complexes at surface sites in comparison with the experiment," *Chem. Rev.*, vol. 94, no. 7, pp. 2095–2160, 1994.

[49] D. McQuarrie, *Statistical Mechanics*. University Science Books, 2000.

[50] S. Choi, J. Drese, and C. Jones, "Adsorbent materials for carbon dioxide capture from large anthropogenic point sources," *ChemSusChem*, vol. 2, no. 9, pp. 796–854, 2009.

[51] K. Dettmer and W. Engewald, "Adsorbent materials commonly used in air analysis for adsorptive enrichment and thermal desorption of volatile organic compounds," *Anal Bioanal Chem.*, vol. 373, no. 6, pp. 490–500, 2002.

[52] J.-R. Li, J. Sculley, and H.-C. Zhou, "Metal–organic frameworks for separations," *Chem. Rev.*, vol. 112, no. 2, pp. 869–932, 2012. PMID: 21978134.

[53] M. Bernal and J. Lopez-Real, "Natural zeolites and sepiolite as ammonium and ammonia adsorbent materials," *Bioresource Technol.*, vol. 43, no. 1, pp. 27 – 33, 1993.

[54] K. Yang and B. Xing, "Adsorption of organic compounds by carbon nanomaterials in aqueous phase: Polanyi theory and its application," *Chem. Rev.*, vol. 110, no. 10, pp. 5989–6008, 2010. PMID: 20518459.

[55] P. Horcajada, R. Gref, T. Baati, P. K. Allan, G. Maurin, P. Couvreur, G. Férey, R. E. Morris, and C. Serre, "Metal–organic frameworks in biomedicine," *Chem. Rev.*, vol. 112, no. 2, pp. 1232–1268, 2012. PMID: 22168547.

[56] J. B. DeCoste and G. W. Peterson, "Metal–organic frameworks for air purification of toxic chemicals," *Chem. Rev.*, vol. 114, no. 11, pp. 5695–5727, 2014. PMID: 24750116.

[57] H. Wu, Q. Gong, D. H. Olson, and J. Li, "Commensurate adsorption of hydrocarbons and alcohols in microporous metal organic frameworks," *Chem. Rev.*, vol. 112, no. 2, pp. 836–868, 2012. PMID: 22257090.

[58] H.-C. Zhou, J. R. Long, and O. M. Yaghi, "Introduction to metal–organic frameworks," *Chem. Rev.*, vol. 112, no. 2, pp. 673–674, 2012. PMID: 22280456.

[59] M. P. Suh, H. J. Park, T. K. Prasad, and D.-W. Lim, "Hydrogen storage in metal–organic frameworks," *Chem. Rev.*, vol. 112, no. 2, pp. 782–835, 2012. PMID: 22191516.

[60] H. Wu, Q. Gong, D. H. Olson, and J. Li, "Commensurate adsorption of hydrocarbons and alcohols in microporous metal organic frameworks," *Chem. Rev.*, vol. 112, no. 2, pp. 836–868, 2012.

[61] K. Bourikas, C. Kordulis, and A. Lycourghiotis, "Titanium dioxide (anatase and rutile): Surface chemistry, liquid–solid interface chemistry, and scientific synthesis of supported catalysts," *Chem. Rev.*, vol. 0, no. 0, p. null, 0. PMID: 25253646.

[62] C. T. Campbell and J. R. V. Sellers, "Enthalpies and entropies of adsorption on well-defined oxide surfaces: Experimental measurements," *Chem. Rev.*, vol. 113, no. 6, pp. 4106–4135, 2013. PMID: 23441680.

[63] H. Chen, C. E. Nanayakkara, and V. H. Grassian, "Titanium dioxide photocatalysis in atmospheric chemistry," *Chem. Rev.*, vol. 112, no. 11, pp. 5919–5948, 2012. PMID: 23088691.

[64] J. Paier, C. Penschke, and J. Sauer, "Oxygen defects and surface chemistry of ceria: Quantum chemical studies compared to experiment," *Chem. Rev.*, vol. 113, no. 6, pp. 3949–3985, 2013. PMID: 23651311.

[65] S. Malinowski, S. Szczepańska, A. Bielański, and J. Sloczyński, "Magnesium oxide as a catalyst: I. acid-base properties of magnesium oxide surface," *J. Catal.*, vol. 4, no. 3, pp. 324 – 331, 1965.

[66] G. Leofanti, M. Solari, G. Tauszik, F. Garbassi, S. Galvagno, and J. Schwank, "Magnesium oxide as a catalyst support: The influence of chlorine," *Appl. Catal.*, vol. 3, no. 2, pp. 131 – 139, 1982.

[67] S. Benedetti, H. Benia, N. Nilius, S. Valeri, and H. Freund, "Morphology and optical properties of MgO thin films on mo(001)," *Chem. Phys. Lett.*, vol. 430, no. 4–6, pp. 330 – 335, 2006.

[68] G. Keller and M. Bhasin, "Synthesis of ethylene via oxidative coupling of methane: I. determination of active catalysts," *J. Catal.*, vol. 73, no. 1, pp. 9 – 19, 1982.

[69] J. S. Lee and S. T. Oyama, "Oxidative coupling of methane to higher hydrocarbons," *Catal. Rev.*, vol. 30, no. 2, pp. 249–280, 1988.

[70] J. H. Lunsford, "The catalytic oxidative coupling of methane," *Angew. Chem. Int. Ed.*, vol. 34, no. 9, pp. 970–980, 1995.

[71] J. V. Smith, "Topochemistry of zeolites and related materials. 1. topology and geometry," *Chem. Rev.*, vol. 88, no. 1, pp. 149–182, 1988.

[72] Y. Li and J. Yu, "New stories of zeolite structures: Their descriptions, determinations, predictions, and evaluations," *Chem. Rev.*, vol. 114, no. 14, pp. 7268–7316, 2014. PMID: 24844459.

[73] D. Barthomeuf, "Basic zeolites: Characterization and uses in adsorption and catalysis," *Catal. Rev.*, vol. 38, no. 4, pp. 521–612, 1996.

[74] A. Corma, "From microporous to mesoporous molecular sieve materials and their use in catalysis," *Chem. Rev.*, vol. 97, no. 6, pp. 2373–2420, 1997. PMID: 11848903.

[75] L. D. Rollmann, E. W. Valyocsik, and R. D. Shannon, *Zeolite Molecular Sieves*, pp. 61–68. John Wiley & Sons, Inc., 2007.

[76] A. Corma, "Inorganic solid acids and their use in acid-catalyzed hydrocarbon reactions," *Chem. Rev.*, vol. 95, no. 3, pp. 559–614, 1995.

[77] F. Sastre, V. Fornés, A. Corma, and H. García, "Selective, room-temperature transformation of methane to C1 oxygenates by deep UV photolysis over zeolites," *J. Am. Chem. Soc.*, vol. 133, no. 43, pp. 17257–17261, 2011.

[78] M. Palomino, A. Corma, F. Rey, and S. Valencia, "New insights on CO_2methane separation using LTA zeolites with different Si/Al ratios and a first comparison with MOFs," *Langmuir*, vol. 26, no. 3, pp. 1910–1917, 2010. PMID: 19757816.

[79] M. Calligaris, G. Nardin, L. Randaccio, and P. C. Chiaramonti, "Cation-site location in a natural chabazite," *Acta Cryst. B*, vol. 38, pp. 602–605, Feb 1982.

[80] L. S. Dent and J. V. Smith, "Crystal structure of chabazite, a molecular sieve," *Nature*, vol. 181, pp. 1794–1796, 06 1958.

[81] R. Barrer, *Hydrothermal Chemistry of Zeolites*. Academic Press, 1982.

[82] M. Iwamoto, S. Yokoo, K. Sakai, and S. Kagawa, "Catalytic decomposition of nitric oxide over copper(II)-exchanged, y-type zeolites," *J. Chem. Soc., Faraday Trans. 1*, vol. 77, pp. 1629–1638, 1981.

[83] W. Quapp and D. Heidrich, "Analysis of the concept of minimum energy path on the potential energy surface of chemically reacting systems," *Theo. Chim. Acta*, vol. 66, no. 3-4, pp. 245–260, 1984.

[84] H. Eyring, "The activated complex in chemical reactions," *J. Chem. Phys.*, vol. 3, no. 2, pp. 107–115, 1935.

[85] M. G. Evans and M. Polanyi, "Some applications of the transition state method to the calculation of reaction velocities, especially in solution," *Trans. Faraday Soc.*, vol. 31, pp. 875–894, 1935.

[86] K. J. Laidler and M. C. King, "Development of transition-state theory," *J. Phys. Chem.*, vol. 87, no. 15, pp. 2657–2664, 1983.

[87] R. Fletcher, *Practical Methods of Optimization: Constrained Optimization*. No. v. 2 in Practical Methods of Optimization: Constrained Optimization, J. Wiley, 1981.

[88] R. Fletcher and C. M. Reeves, "Function minimization by conjugate gradients," *Comput. J.*, vol. 7, no. 2, pp. 149–154, 1964.

[89] P. Császár and P. Pulay, "Geometry optimization by direct inversion in the iterative subspace," *J. Mol. Struct.*, vol. 114, no. 0, pp. 31–34, 1984.

[90] R. Judson, *Genetic Algorithms and Their Use in Chemistry*, pp. 1–73. John Wiley & Sons, Inc., 2007.

[91] H. B. Schlegel, "Geometry optimization," *WIREs Comput Mol Sci*, vol. 1, no. 5, pp. 790–809, 2011.

[92] J. E. Bright Wilson, J. Decius, and P. . . Cross, *Molecular Vibrations*. Dover Publ., 1955.

[93] P. Pulay, "Ab initio calculation of force constants and equilibrium geometries in polyatomic molecules," *Mol. Phys.*, vol. 17, no. 2, pp. 197–204, 1969.

[94] H. Horn, H. Weiß, M. Háser, M. Ehrig, and R. Ahlrichs, "Prescreening of two-electron integral derivatives in scf gradient and hessian calculations," *J. Comput. Chem.*, vol. 12, no. 9, pp. 1058–1064, 1991.

[95] P. Deglmann, K. May, F. Furche, and R. Ahlrichs, "Nuclear second analytical derivative calculations using auxiliary basis set expansions," *Chem. Phys. Lett.*, vol. 384, no. 1–3, pp. 103 – 107, 2004.

[96] P. Bouř and T. A. Keiderling, "Partial optimization of molecular geometry in normal coordinates and use as a tool for simulation of vibrational spectra," *J. Chem. Phys.*, vol. 117, no. 9, pp. 4126–4132, 2002.

[97] A. Banerjee, N. Adams, J. Simons, and R. Shepard, "Search for stationary points on surfaces," *J. Phys. Chem.*, vol. 89, pp. 52–57, 2012/11/19 1985.

[98] C. G. Broyden, "The convergence of a class of double-rank minimization algorithms 1. general considerations," *J. Appl. Math.*, vol. 6, no. 1, pp. 76–90, 1970.

[99] R. Fletcher, "A new approach to variable metric algorithms," *Comput. J.*, vol. 13, no. 3, pp. 317–322, 1970.

[100] D. Goldfarb, "A family of variable-metric methods derived by variational means," *Math. Comput.*, vol. 24, no. 109, p. 23, 1970.

[101] D. F. Shanno, "Conditioning of quasi-newton methods for function minimization conditioning of quasi-newton methods for function minimization," *Math. Comput.*, vol. 24, no. 111, p. 647, 1970.

[102] R. Fletcher and M. J. D. Powell, "A rapidly convergent descent method for minimization," *Comput. J.*, vol. 6, no. 2, pp. 163–168, 1963.

[103] C. Eckart, "The kinetic energy of polyatomic molecules," *Phys. Rev.*, vol. 46, pp. 383–387, 09 1934.

[104] B. Fornberg, "Generation of finite-difference formulas on arbitrarily spaced grids," *Math. Comput.*, vol. 51, pp. 699–706, Oct 1988.

[105] Y. Panchenko, V. Pupyshev, and C. Bock, "Vibrational anharmonicity and scaling the quantum mechanical molecular force field," *J. Mol. Struct.*, vol. 550–551, no. 0, pp. 495 – 504, 2000.

[106] R. Levine, "Representation of one-dimensional motion in a morse potential by a quadratic hamiltonian," *Chem. Phys. Lett.*, vol. 95, no. 2, pp. 87 – 90, 1983.

[107] L. Sprandel and C. Kern, "A test of perturbation theory for determining anharmonic vibrational corrections to properties of diatomic molecules," *Mol. Phys.*, vol. 24, no. 6, pp. 1383–1391, 1972.

[108] J. M. Bowman, "The self-consistent-field approach to polyatomic vibrations," *Acc. Chem. Res.*, vol. 19, no. 7, pp. 202–208, 1986.

[109] O. Christiansen and J. M. Luis, "Beyond vibrational self-consistent-field methods: Benchmark calculations for the fundamental vibrations of ethylene," *Int. J. Quant. Chem.*, vol. 104, no. 5, pp. 667–680, 2005.

[110] M. B. Hansen, O. Christiansen, D. Toffoli, and J. Kongsted, "A virtual vibrational self-consistent-field method for efficient calculation of molecular vibrational partition functions and thermal effects on molecular properties," *J. Chem. Phys.*, vol. 128, no. 17, pp. –, 2008.

[111] V. Bakken and T. Helgaker, "The efficient optimization of molecular geometries using redundant internal coordinates," *J. Chem. Phys.*, vol. 117, no. 20, pp. 9160–9174, 2002.

[112] J. Andzelm, R. King-Smith, and G. Fitzgerald, "Geometry optimization of solids using delocalized internal coordinates," *Chem. Phys. Lett.*, vol. 335, no. 3–4, pp. 321 – 326, 2001.

[113] K. N. Kudin, G. E. Scuseria, and H. B. Schlegel, "A redundant internal coordinate algorithm for optimization of periodic systems," *J. Chem. Phys.*, vol. 114, no. 7, pp. 2919–2923, 2001.

[114] T. Bučko, J. Hafner, and J. G. Ángyán, "Geometry optimization of periodic systems using internal coordinates," *J. Chem. Phys.*, vol. 122, no. 12, pp. –, 2005.

[115] P. Y. Ayala and H. B. Schlegel, "Identification and treatment of internal rotation in normal mode vibrational analysis," *J. Chem. Phys.*, vol. 108, no. 6, pp. 2314–2325, 1998.

[116] Z. Konkoli and D. Cremer, "A new way of analyzing vibrational spectra. i. derivation of adiabatic internal modes," *Int. J. Quant. Chem.*, vol. 67, no. 1, pp. 1–9, 1998.

[117] Z. Konkoli, J. A. Larsson, and D. Cremer, "A new way of analyzing vibrational spectra. II. comparison of internal mode frequencies," *Int. J. Quant. Chem.*, vol. 67, no. 1, pp. 11–27, 1998.

[118] Z. Konkoli and D. Cremer, "A new way of analyzing vibrational spectra. III. characterization of normal vibrational modes in terms of internal vibrational modes," *Int. J. Quant. Chem.*, vol. 67, no. 1, pp. 29–40, 1998.

[119] Z. Konkoli, J. A. Larsson, and D. Cremer, "A new way of analyzing vibrational spectra. IV. application and testing of adiabatic modes within the concept of the characterization of normal modes," *Int. J. Quant. Chem.*, vol. 67, no. 1, pp. 41–55, 1998.

[120] F. Jensen and D. S. Palmer, "Harmonic vibrational analysis in delocalized internal coordinates," *J. Chem. Theory Comput.*, vol. 7, no. 1, pp. 223–230, 2011.

[121] J. Baker, A. Kessi, and B. Delley, "The generation and use of delocalized internal coordinates in geometry optimization," *J. Chem. Phys.*, vol. 105, no. 1, pp. 192–212, 1996.

[122] J. Baker and P. Pulay, "Geometry optimization of atomic microclusters using inversepower distance coordinates," *J. Chem. Phys.*, vol. 105, no. 24, pp. 11100–11107, 1996.

[123] J. Baker, D. Kinghorn, and P. Pulay, "Geometry optimization in delocalized internal coordinates: An efficient quadratically scaling algorithm for large molecules," *J. Chem. Phys.*, vol. 110, no. 11, pp. 4986–4991, 1999.

[124] P. Pulay and G. Fogarasi, "Geometry optimization in redundant internal coordinates," *J. Chem. Phys.*, vol. 96, no. 4, pp. 2856–2860, 1992.

[125] P. Hohenberg and W. Kohn, "Inhomogeneous electron gas," *Phys. Rev.*, vol. 136, pp. B864–B871, Nov 1964.

[126] W. Kohn and L. J. Sham, "Self-consistent equations including exchange and correlation effects," *Phys. Rev.*, vol. 140, pp. A1133–A1138, Nov 1965.

[127] W. Kohn, A. D. Becke, and R. G. Parr, "Density functional theory of electronic structure," *The Journal of Physical Chemistry*, vol. 100, no. 31, pp. 12974–12980, 1996.

[128] R. Parr and W. Yang, *Density-Functional Theory of Atoms and Molecules*. International Series of Monographs on Chemistry, Oxford University Press, USA, 1989.

[129] A. D. Becke, "Density-functional exchange-energy approximation with correct asymptotic behavior," *Phys. Rev. A*, vol. 38, pp. 3098–3100, Sep 1988.

[130] S. Grimme, "Semiempirical GGA-type density functional constructed with a long-range dispersion correction," *J. Comput. Chem.*, vol. 27, no. 15, pp. 1787–1799, 2006.

[131] C. Tuma and J. Sauer, "A hybrid MP2/planewave-DFT scheme for large chemical systems: Proton jumps in zeolites," *Chem. Phys. Lett.*, vol. 387, no. 4–6, pp. 388 – 394, 2004.

[132] C. Tuma and J. Sauer, "Treating dispersion effects in extended systems by hybrid MP2:DFT calculations-protonation of isobutene in zeolite ferrierite," *Phys. Chem. Chem. Phys.*, vol. 8, pp. 3955–3965, 2006.

[133] C. Møller and M. S. Plesset, "Note on an approximation treatment for many-electron systems," *Phys. Rev.*, vol. 46, pp. 618–622, Oct 1934.

[134] "TURBOMOLE V6.2 2010, a development of University of Karlsruhe and Forschungszentrum Karlsruhe GmbH, 1989-2007, TURBOMOLE GmbH, since 2007; available from `http://www.turbomole.com`.."

[135] C. Hättig and F. Weigend, "CC2 excitation energy calculations on large molecules using the resolution of the identity approximation," *J. Chem. Phys.*, vol. 113, no. 13, pp. 5154–5161, 2000.

[136] F. Weigend and M. Häser, "RI-MP2: First derivatives and global consistency," *Theo. Chem. Acc.*, vol. 97, no. 1-4, pp. 331–340, 1997.

[137] U. Eichler, C. M. Kölmel, and J. Sauer, "Combining ab initio techniques with analytical potential functions for structure predictions of large systems: Method and application to crystalline silica polymorphs," *J. Comput. Chem.*, vol. 18, no. 4, pp. 463–477, 1997.

[138] J. Sauer and M. Sierka, "Combining quantum mechanics and interatomic potential functions in ab initio studies of extended systems," *J. Comput. Chem.*, vol. 21, no. 16, pp. 1470–1493, 2000.

[139] S. Boys and F. Bernardi, "The calculation of small molecular interactions by the differences of separate total energies. some procedures with reduced errors," *Mol. Phys.*, vol. 19, no. 4, pp. 553–566, 1970.

[140] T. H. Dunning, "Gaussian basis sets for use in correlated molecular calculations. i. the atoms boron through neon and hydrogen," *J. Chem. Phys.*, vol. 90, no. 2, pp. 1007–1023, 1989.

[141] A. Halkier, W. Klopper, T. Helgaker, P. Jo/rgensen, and P. R. Taylor, "Basis set convergence of the interaction energy of hydrogen-bonded complexes," *J. Chem. Phys.*, vol. 111, no. 20, pp. 9157–9167, 1999.

[142] A. Halkier, T. Helgaker, P. Jørgensen, W. Klopper, and J. Olsen, "Basis-set convergence of the energy in molecular hartree–fock calculations," *Chem. Phys. Lett.*, vol. 302, no. 5–6, pp. 437 – 446, 1999.

[143] F. Jensen, "On the accuracy of numerical hartree–fock energies," *Theo. Chem. Acc.*, vol. 113, no. 3, pp. 187–190, 2005.

[144] T. Helgaker, W. Klopper, H. Koch, and J. Noga, "Basis-set convergence of correlated calculations on water," *J. Chem. Phys.*, vol. 106, no. 23, pp. 9639–9646, 1997.

[145] P. E. Blöchl, "Projector augmented-wave method," *Phys. Rev. B*, vol. 50, pp. 17953–17979, Dec 1994.

[146] G. Kresse and D. Joubert, "From ultrasoft pseudopotentials to the projector augmented-wave method," *Phys. Rev. B*, vol. 59, pp. 1758–1775, Jan 1999.

[147] H. J. Monkhorst and J. D. Pack, "Special points for brillouin-zone integrations," *Phys. Rev. B*, vol. 13, pp. 5188–5192, Jun 1976.

[148] J. P. Perdew, J. A. Chevary, S. H. Vosko, K. A. Jackson, M. R. Pederson, D. J. Singh, and C. Fiolhais, "Atoms, molecules, solids, and surfaces: Applications of the generalized gradient approximation for exchange and correlation," *Phys. Rev. B*, vol. 46, p. 6671, 1992.

[149] M. Brändle, J. Sauer, R. Dovesi, and N. M. Harrison, "Comparison of a combined quantum mechanics/interatomic potential function approach with its periodic quantum-mechanical limit: Proton siting and ammonia adsorption in zeolite chabazite," *J. Chem. Phys.*, vol. 109, no. 23, pp. 10379–10389, 1998.

[150] T. Kerber, M. Sierka, and J. Sauer, "Application of semiempirical long-range dispersion corrections to periodic systems in density functional theory," *J. Comput. Chem.*, vol. 29, no. 13, pp. 2088–2097, 2008.

[151] D. E. Woon and T. H. Dunning, "Gaussian basis sets for use in correlated molecular calculations. III. the atoms aluminum through argon," *J. Chem. Phys.*, vol. 98, no. 2, pp. 1358–1371, 1993.

[152] S. E. Stein and B. S. Rabinovitch, "Accurate evaluation of internal energy level sums and densities including anharmonic oscillators and hindered rotors," *J. Chem. Phys.*, vol. 58, no. 6, pp. 2438–2445, 1973.

[153] A. Warshel, "Calculation of the anharmonicity in the vibrational frequencies of alkane molecules by the CFF functions," *J. Chem. Phys.*, vol. 55, no. 7, pp. 3327–3335, 1971.

[154] A. Chakraborty and D. G. Truhlar, "Converged vibrational energy levels and quantum mechanical vibrational partition function of ethane," *J. Chem. Phys.*, vol. 124, no. 18, pp. –, 2006.

[155] B. Kirtman, W. E. Palke, and C. S. Ewig, "Effect of vibrations on the internal rotation barrier in ethane," *J. Chem. Phys.*, vol. 64, no. 5, pp. 1883–1890, 1976.

[156] L. S. Bartell, S. Fitzwater, and W. J. Hehre, "Representations of molecular force fields. i. ethane: Abinitio and model, harmonic and anharmonic," *J. Chem. Phys.*, vol. 63, no. 11, pp. 4750–4758, 1975.

[157] T. Shimanouchi, *Tables of Molecular Vibrational Frequencies*. No. v. 1 in NSRDS-NBS, National Bureau of Standards, 1972.

[158] B. Smit and T. L. M. Maesen, "Molecular simulations of zeolites: Adsorption, diffusion, and shape selectivity," *Chem. Rev.*, vol. 108, no. 10, pp. 4125–4184, 2008.

[159] G. J. Kramer, R. A. van Santen, C. A. Emels, and A. K. Novak, "Understanding the acid behaviour of zeolites from theory and experiment," *Nature*, vol. 363, pp. 529–531, 1993.

[160] A. Ghysels, D. V. Neck, V. V. Speybroeck, T. Verstraelen, and M. Waroquier, "Vibrational modes in partially optimized molecular systems," *J. Chem. Phys.*, vol. 126, no. 22, p. 224102, 2007.

[161] A. M. Hofmeister, E. Keppel, and A. K. Speck, "Absorption and reflection infrared spectra of MgO and other diatomic compounds," *MNRAS*, vol. 345, no. 1, pp. 16–38, 2003.

[162] R. Hanna, "Infrared properties of magnesium oxide," *J. Am. Ceram. Soc.*, vol. 48, no. 7, pp. 376–380, 1965.

[163] S. P. Bates, W. J. M. van Well, R. A. van Santen, and B. Smit, "Energetics of n-alkanes in zeolites: a configurational-bias monte carlo investigation into pore size dependence," *J. Am. Chem. Soc.*, vol. 118, no. 28, pp. 6753–6759, 1996.

[164] F. Eder, M. Stockenhuber, and J. A. Lercher, "Brønsted acid site and pore controlled siting of alkane sorption in acidic molecular sieves," *J. Phys. Chem. B*, vol. 101, no. 27, pp. 5414–5419, 1997.

Acknowledgements

I thank Prof. Dr. Joachim Sauer for the opportunity to work in his group and for giving me his advice, suggestions, and criticism.

I thank all the group members for helping in different stages of this work.

I thank the "International Max Planck Research School" (IMPRS) on Functional Interfaces in Physics and Chemistry for building collaborative scientific interactions among different surface science fields and for funding.

I thank the "Verband der Chemischen Industrie" for a Kekulé stipend.

I finally thank the "North German Computing Alliance Berlin - Hannover" (HLRN) for a computer grant and relative technical support (Dr. Christian Tuma and Dr. Jens Döbler).

Selbstständigkeitserklärung

Hiermit erkläre ich, dass ich die vorliegende Dissertation selbstständig und nur unter Verwendung der angegebenen Literatur und Hilfsmittel angefertigt habe.

GiovanniMaria Piccini